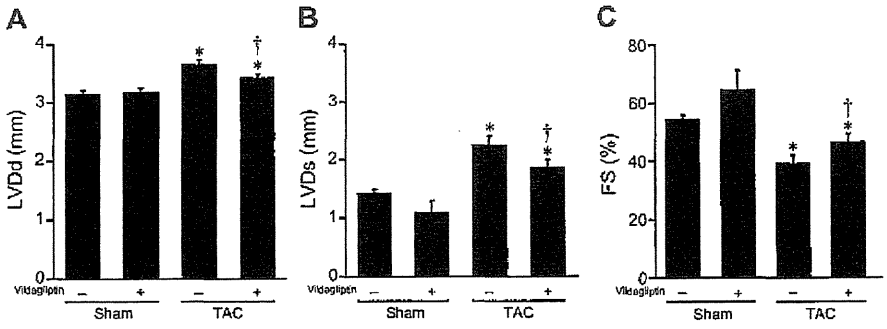

Fig. 3. *A* and *B*: left ventricular (LV) dimensions. *C*: fractional shortening (FS) 4 wk after TAC or sham operation. LV end-diastolic diameter (Dd), end-systolic diameter (Ds), and FS measured by echocardiography at 4 wk after TAC or sham operation. Echocardiographic analysis revealed enlarged LV end-diastolic and end-systolic diameters in both of the TAC groups compared with the sham-operated mice. Both LV dilatation and dysfunction in the TAC group were ameliorated by vildagliptin treatment. Sham-operated mice (n = 5), sham-operated mice with vildagliptin (n = 5), TAC mice (n = 17), and TAC mice with vildagliptin (n = 27) were examined. LVDd, LV end-diastolic dimension; LVDs, LV end-systolic dimension. Data shown are means ± SE. *P < 0.05 vs. sham operated, †P < 0.05 vs. TAC.

Water uptake and heart weight. Body weight was not statistically different between the groups: 24.3 ± 1.7 g and 23.4 ± 1.4 g in the sham-operated and TAC mice without vildagliptin (n = 10 and 17), 25.8 ± 1.7 g and 25.2 ± 2.4 g in the sham-operated and TAC mice with vildagliptin (n =10 and 27). Heart weight-to-body weight ratio (HW/BW) markedly increased in the TAC group compared with the sham-operated group (4.9 ± 0.1 vs. 9.3 ± 0.5 for sham-operated and TAC mice without vildagliptin, respectively; P < 0.05), and vildagliptin did not attenuate HW/BW (9.2 ± 0.4 for TAC with vildagliptin; Fig. 4). Volumes of vildagliptin solution or water consumed were similar in all of the groups (5.2 ± 0.2, 4.9 ± 0.5, 4.4 ± 0.9, and 4.5 ± 1.3 ml/day for sham-operated with and without vildagliptin and TAC with and without vildagliptin, respectively; $P \geq 0.05$ for all).

Apoptosis and fibrosis. We performed TUNEL staining to clarify the degree of apoptosis in the murine hearts. Apoptosis in the myocardium of the TAC mice was increased compared with the sham-operated mice, and this increase in apoptotic cell death was largely attenuated by vildagliptin (Fig. 5, *A* and *B*, n = 4 per each group). Next we performed immunoblotting to confirm apoptotic changes in protein levels. We observed increased cleaved caspase-3 protein in pressure-overloaded murine hearts, which was partially ameliorated by vildagliptin

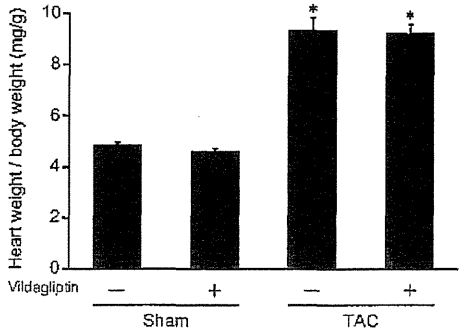

Fig. 4. Heart weight (mg)/body wt (g) ratio 4 wk after the TAC or sham operation. Sham-operated mice (n = 10), sham-operated mice with vildagliptin (n = 10), TAC mice (n = 17), and TAC mice with vildagliptin (n = 27) mice were measured. The values shown are means ± SE. *P < 0.05 vs. sham operated.

(Fig. 5, *C* and *D*, n = 4 per each group). These findings indicate that vildagliptin partly reduces myocardial apoptosis in pressure-overloaded murine hearts.

Figure 6*A* shows increases in myocardial collagen in the TAC group, also ameliorated by vildagliptin. Figures 6*B* shows fibrotic areas identified by picrosirius red staining. The total myocardial interstitial collagen area significantly increased in the TAC group compared with the sham-operated groups (P < 0.05 vs. sham operated, n = 5 per each group) but was decreased in the TAC with vildagliptin group (P < 0.05 vs. TAC) (sham operated, 1.79 ± 0.22%; sham operated with vildagliptin, 1.77 ± 0.20%; TAC, 12.12 ± 0.27%; TAC with vildagliptin, 8.02 ± 1.84%). We next analyzed expression of *Tgf-1β*, a fibrosis-related gene, using RT-PCR. Myocardial *Tgf-1β* expression significantly increased in the TAC group compared with that in the sham-operated group (P < 0.05 vs. sham operated) but significantly decreased in the groups with vildagliptin (P < 0.05 vs. TAC; sham operated, 1 ± 0.08; sham operated with vildagliptin, 0.98 ± 0.11; TAC, 1.85 ± 0.12; TAC with vildagliptin, 1.55 ± 0.06; Fig. 6*C*, n = 3 per each group).

Finally, we performed immunoblotting to verify the fibrotic changes that arose through increased levels of TGF-β pathway proteins. We observed increased p-Smad2 and p-Smad3 protein levels in the pressure-overloaded murine hearts, which were partially restored by vildagliptin (Fig. 7, n = 4 per each group). These findings indicate that vildagliptin reverses myocardial fibrosis via the TGF-β pathway in murine pressure-overloaded hearts.

Survival analysis. The number of TAC mice without vildagliptin was 41 and the number of those with vildagliptin was 40. Only 17 (41.5%) TAC mice without vildagliptin survived 28 days, whereas 27 (67.5%) TAC mice with vildagliptin survived 28 days (Fig. 8; P < 0.05). These data indicate that vildagliptin treatment is strongly protective. Vildagliptin did not affect the survival rate in the sham-operated mice.

DISCUSSION

This study was the first to demonstrate that a DPP-IV inhibitor improved survival rate in mice with pressure-overloaded HF. We presented the following experimental evidence: *1*) TAC exacerbated the development of impaired glucose

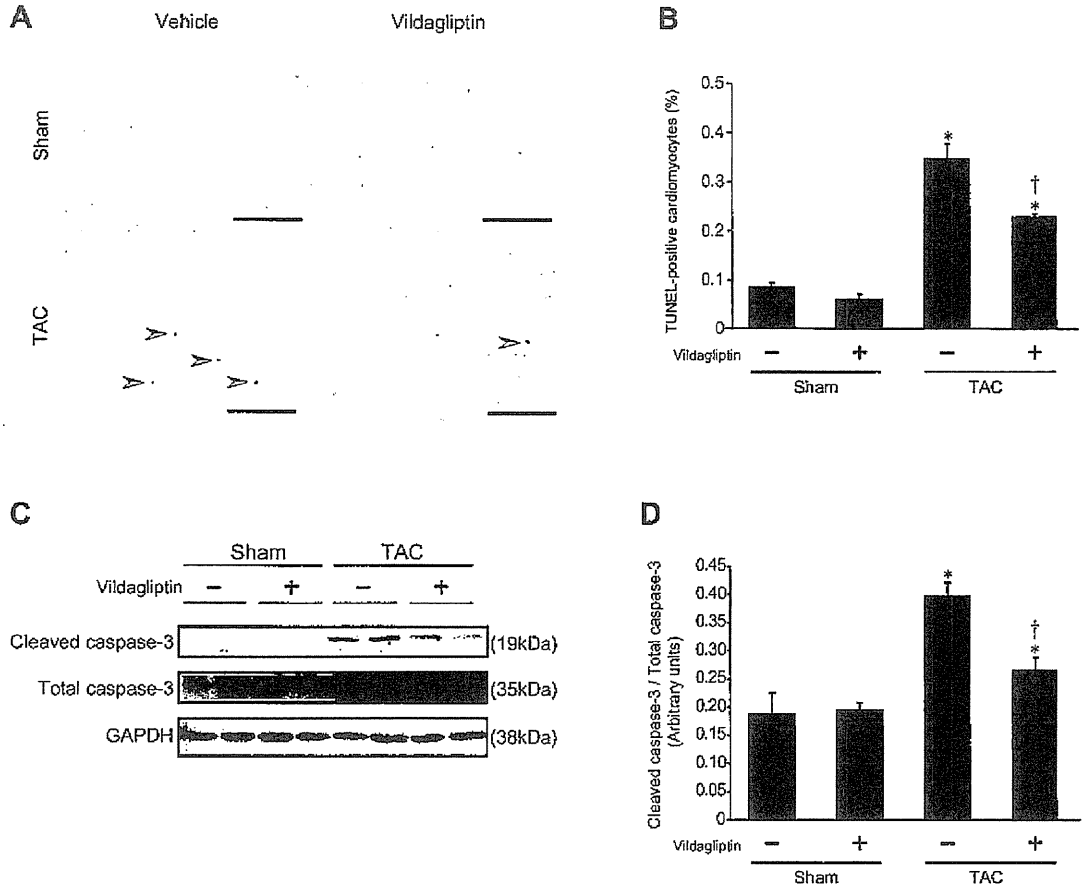

Fig. 5. *A*: representative images of the terminal deoxynucleotidyl transferase dUTP nick-end labeling (TUNEL)-positive cells in murine hearts. Top left, sham operated; top right, sham operated with vildagliptin; bottom left, TAC; bottom right, TAC with vildagliptin. Evidence of apoptosis, including chromatin condensation, is indicated with arrowheads. The proportion of TAC-induced apoptotic cells was decreased by vildagliptin. Bar = 200 μm; original magnification, ×200. *B*: quantitative analysis of murine apoptotic cardiomyocytes. TAC increased the number of apoptotic cells in the myocardium compared with the sham-operated group, and vildagliptin attenuated the increase in apoptosis. $n = 4$ for each group. *C*: representative immunoblotting analysis of cleaved/total caspase-3 and GAPDH in the hearts of sham-operated and TAC mice with or without vildagliptin. *D*: intensity of bands was quantified from four independent experiments by densitometry. Cleaved/total caspase-3 protein levels were increased by pressure overload in the hearts of TAC mice, which were reversed in TAC mice with vildagliptin. $n = 4$ for each group. The values shown are means ± SE. $^*P < 0.05$ vs. sham operated, $\dagger P < 0.05$ vs. TAC.

tolerance, which was attenuated by vildagliptin with an attendant increase in total GLP-1 levels; *2*) TAC induced myocardial apoptosis and fibrosis, which were attenuated by vildagliptin; *3*) TAC increased LVDd and LVDs, leading to FS decline, while vildagliptin attenuated increased LVDd and LVDs and increased LVFS. These effects may contribute to the improvement in survival rate generated by vildagliptin in mice with pressure overload-induced HF.

We demonstrated that TAC exacerbated the development of impaired glucose tolerance, which was attenuated by vildagliptin. This result implies that HF causes impaired glucose tolerance and improvement of impaired glucose tolerance may ameliorate HF severity. Glycemic control independently correlates with reduced LV contractile reserve and positivity for HF in diabetic patients (12, 28). We previously reported that HF is associated with impaired glucose tolerance in mice and dogs, and that correction of impaired glucose tolerance with voglibose or metformin reduces HF severity (26, 27, 41). Shimizu et al. (46) reported that systolic dysfunction induced by pressure overload exacerbates plasma glucose and hepatic insulin resistance via Akt and insulin signaling in rodents. In humans, chronic HF is associated with hyperinsulinemia (36, 51). Insulin resistance observed in HF is partly due to the lack of activity and increase in weight gain/fat redistribution. Stolen et al. (49) showed that exercise training improved insulin-stimulated myocardial glucose uptake in patients with dilated cardiomyopathy. Ashrafian et al. (2) proposed the other mechanism of HF-induced insulin resistance. Hyperadrenergic state of HF initiates the elevation of plasma free fatty acids (FFAs). The elevation of plasma FFAs induces insulin resistance due to increased triglycerides, increased cellular FFAs, and increased cytoplasmic fatty acid metabolites in hearts and skeletal muscle (43).

To our knowledge, this is the first study to evaluate an improvement in impaired glucose tolerance in animals with HF in the presence of DPP-IV inhibitors. Indeed, vildagliptin increased the plasma GLP-1 levels in animals with TAC-induced HF, suggesting that HF is attenuated by the correction

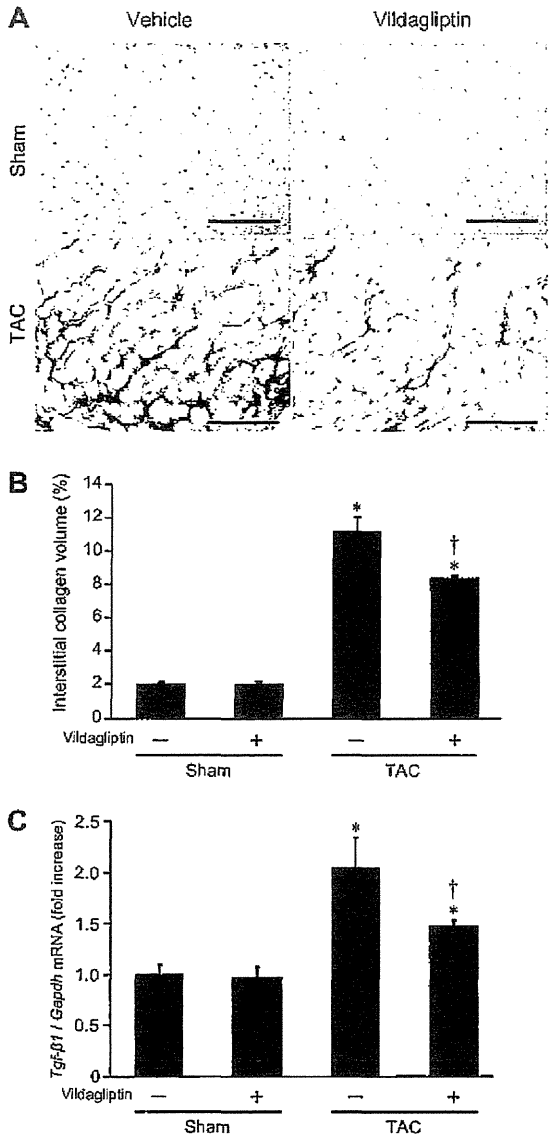

Fig. 6. *A*: representative images of the murine myocardium stained by picrosirius red. Collagen accumulation induced by TAC was regressed with vildagliptin. Top left, sham operated; top right, sham operated with vildagliptin; bottom left, TAC; bottom right, TAC with vildagliptin. Bar = 100 μm; original magnification, ×400. *B*: quantitative analysis shows that vildagliptin ameliorated myocardial collagen deposition resulting from pressure overload. $n = 5$ for each group. *C*: quantitative analysis of *transforming growth factor-1 β (Tgfl β)* in murine hearts: the expression level (normalized to *Gapdh*) in TAC group was increased compared with that in sham operated, which was alleviated in TAC with vildagliptin. $n = 3$ for each group. Data are presented as the relative change vs. sham operated. The values shown are means ± SE. $*P < 0.05$ vs. sham operated, $\dagger P < 0.05$ vs. TAC.

of glucose intolerance by DPP-IV inhibitors. This hypothesis is supported by our findings that vildagliptin attenuates LV apoptosis and fibrosis in the TAC mice, which may explain the amelioration of LV dilatation and dysfunction. This evidence is consistent with previous studies in which sitagliptin was shown to attenuate HF severity induced by rapid pacing in pigs (14), ameliorate myocardial fibrosis in diabetic ($db/db^{-/-}$) mice (23), and improve diastolic dysfunction without altering ejection fraction in a rat model of uremic cardiomyopathy (9).

Intriguingly, GLP-1 reportedly has cardioprotective properties besides its ability to correct glucose intolerance in HF. GLP-1 receptors are expressed in the heart and activate PI3 kinase and Akt in addition to cyclic AMP (6, 19). Protein kinase A activation via accumulation of cyclic AMP may activate p38 MAP kinase, which may in turn mediate cardio-

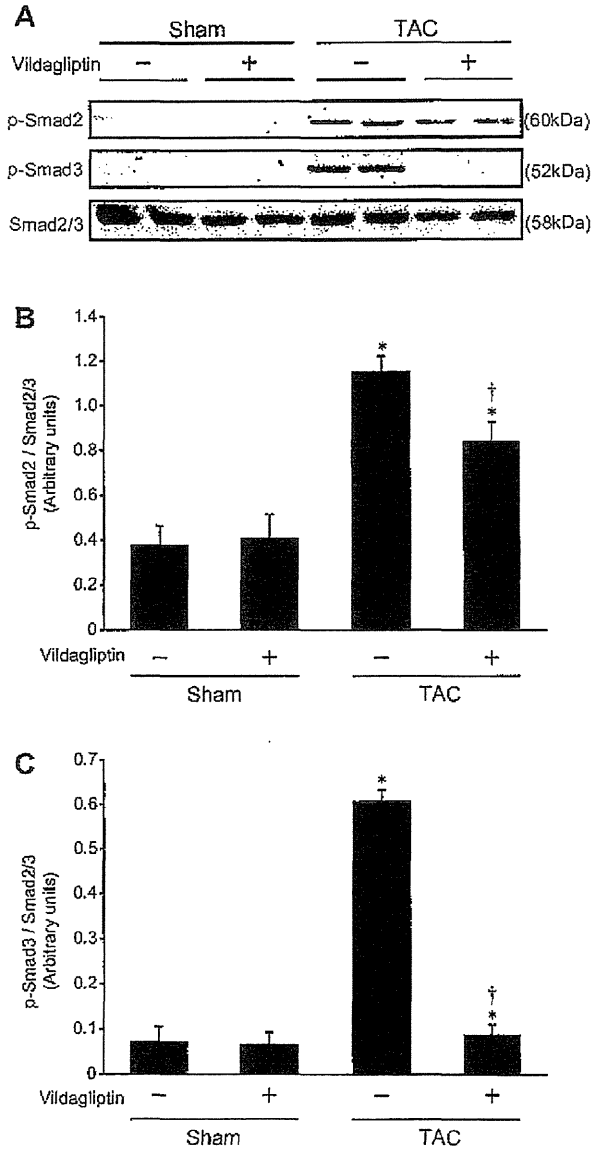

Fig. 7. *A*: representative immunoblotting analysis of phosphorylated Smad2 (p-Smad2), p-Smad3, and Smad2/3 in the hearts of sham-operated and TAC mice with or without vildagliptin. *B*: band intensity quantified by densitometry. p-Smad2/Smad2/3 protein levels increased as a result of pressure overload in the hearts of TAC mice, but recovered in TAC mice with vildagliptin. *C*: band intensity quantified by densitometry. p-Smad3/Smad2/3 protein levels increased as a result of pressure overload in the hearts of the TAC mice, but recovered in the TAC mice with vildagliptin. $n = 4$ for each group. The values shown are means ± SE. $*P < 0.05$ vs. sham operated, $\dagger P < 0.05$ vs. TAC.

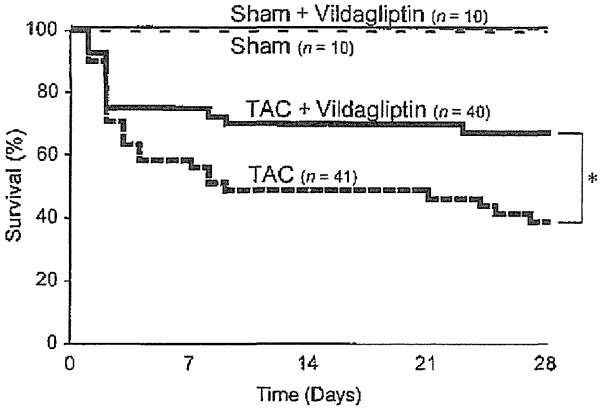

Fig. 8. The Kaplan-Meier curve analysis shows that the TAC group with vildagliptin exhibited improved survival compared with the TAC group without vildagliptin. We enrolled 41 mice in the TAC and 40 mice in the TAC with vildagliptin groups, respectively. The survival rates at 28 days after the TAC operation were 41.5% (17/41) in the TAC and 67.5% (27/40) in the TAC with vildagliptin groups, respectively. *$P < 0.05$ vs. TAC; *n*, number of mice.

protection (40, 59), and activation of PI3 kinase and Akt may further enhance these cardioprotective effects. A recent report (55) demonstrated amelioration of nonalcoholic steatohepatitis in mice by an analog of exenatide, a GLP-1 receptor agonist, supporting the antifibrotic effect of GLP-1 in murine hearts. Indeed, GLP-1 administration in patients with HF decreased the HF severity with or without DM, suggesting that GLP-1 may have cardioprotective properties independent of its effects on blood glucose levels (48). However, GLP-1 levels were elevated ~10-fold (17), significantly higher than the GLP-1 levels observed with DPP-IV inhibitors (4), suggesting that even a 1-pM increase in GLP-1 may be sufficient for cardioprotection. Moreover, in a large meta-analysis, vildagliptin was not associated with an increased risk of adjudicated cardio- and cerebrovascular events relative to all comparators in the patients with type 2 diabetes, including increased cerebrovascular risks (44). Chaykovska et al. (9) showed that increased *Tgf-β1*, *collagen type I α1*, and *collagen type III α1* expression in uremic rat hearts, compared with the sham-operated rat hearts, was significantly reduced by linagliptin, a DPP-IV inhibitor, supporting our observations. Importantly, DPP-IV inhibitors impact cardioprotection independently of GLP-1; DPP-IV also reportedly degrades peptides tyrosine-tyrosine, stromal cell-derived factor-1, and B-type natriuretic peptide (BNP) (7, 32, 45, 47). Taken together, these data suggest that DPP-IV inhibitors are cardioprotective, suggesting that they may also be beneficial for patients with HF. However, this hypothesis is limited because we used 8-wk-old mice with TAC as a model of HF in this study. Although this model is one of established animal models for HF, this model is not the universal model for the patients with HF, or does not mimic the background of the HF patients (e.g., age, dyslipidemia, ischemia, etc.). Further basic and preclinical studies are needed to apply DPP-IV inhibitors to HF patients.

The most important issue in this study was to determine whether DPP-IV inhibitors increase the survival rate because improvements in HF do not necessarily increase the survival rate. Indeed, inotropic agents such as phosphodiesterase III inhibitors (e.g., vesnarinone) improved pathophysiological parameters of HF in basic studies, even improving symptoms and cardiac function in patients with HF in clinical studies, but these drugs actually decreased the patient survival rate in large-scale clinical trials (10). This unexpected finding is attributable to the fact that the effect of these drugs on survival rate was never tested in experimental models of chronic HF. Yin et al. (60) reported the rat models with the administration of vildagliptin 2 days before or 3 wk after acute myocardial infarction surgery. They did not show the cardiac contractility and survival or any change in glucose metabolism with vildagliptin treatment. Compared with their protocol, we administered vildagliptin from 1 day postsurgery of murine TAC, which finally reversed the survival rate. These discrepancies between the study of Yin et al. and our present study may be attributable to the manner of HF induction (e.g., models and species), their glucose levels, and the dosage of vildagliptin. Their echocardiographic data seem to show worse HF than ours, which was too severe to treat with their dose set. In addition, although they did not mention any condition of the feeding (e.g., fasting or ad libitum feeding) during sampling, no difference in their blood glucose levels may suggest that the dosage was not enough to be cardioprotective. We observed that vildagliptin increased survival rate in the context of pressure overload-induced HF in mice, indicating that an adequate dose of DPP-IV inhibitors is ultimately cardioprotective against HF.

This study includes the limitations. Since TAC animals are fragile, especially when using the narrower size of needle (30 gauge) to create severe HF, the procedures of the examination such as glucose tolerance test may worsen the HF of the TAC mice. Indeed, in the preliminary study, we tried to perform oral glucose tolerance test at first, but 2 of 6 died because of the onset of acute severe HF (pulmonary edema shown by dissection). This is the reason that we shifted to the intraperitoneal glucose tolerance test, which did not cause severe HF leading to death. Importantly, the timing and number of procedures were identical in the groups with or without vildagliptin, suggesting that these additional stresses of examination to TAC do not largely affect the present results and conclusions.

In conclusion, vildagliptin, a DPP-IV inhibitor, improved the pathophysiology of HF in pressure-overloaded mice. This effect was mediated partly by improved glucose tolerance and partly by the cardioprotective effects of GLP-1, both of which ultimately improved survival following HF.

ACKNOWLEDGMENTS

We are thankful to Akiko Ogai, Chizuko Kimura, and Nobuyoshi Imai for excellent technical assistance. Vildagliptin was a gift from Novartis.

GRANTS

This work was supported by grants-in-aid from the Ministry of Health, Labor, and Welfare of Japan and the Ministry of Education, Culture, Sports, Science and Technology of Japan.

DISCLOSURES

No conflicts of interest, financial or otherwise, are declared by the author(s).

AUTHOR CONTRIBUTIONS

Author contributions: A.T., M.A., and M.K. conception and design of research; A.T., S.I., Y.Y., and Y.L. performed experiments; A.T., S.Y., and M.K. analyzed data; A.T., S.I., K.-D.M., K.S., and Y.Y. prepared figures; A.T. drafted manuscript; A.T., S.I., K.-D.M., K.S., S.S., Y.A., S.T., T.M., and H.A.

edited and revised manuscript; S.I., K.-D.M., Y.L., H.I.-U., and M.K. interpreted results of experiments; N.M. and M.K. approved final version of manuscript.

REFERENCES

1. **Abhayaratna WP, Marwick TH, Smith WT, Becker NG.** Characteristics of left ventricular diastolic dysfunction in the community: an echocardiographic survey. *Heart* 92: 1259–1264, 2006.
2. **Ashrafian H, Frenneaux MP, Opie LH.** Metabolic mechanisms in heart failure. *Circulation* 116: 434–448, 2007.
3. **Ban K, Noyan-Ashraf MH, Hoefer J, Bolz SS, Drucker DJ, Husain M.** Cardioprotective and vasodilatory actions of glucagon-like peptide 1 receptor are mediated through both glucagon-like peptide 1 receptor-dependent and -independent pathways. *Circulation* 117: 2340–2350, 2008.
4. **Bergman AJ, Stevens C, Zhou Y, Yi B, Laethem M, De Smet M, Snyder K, Hilliard D, Tanaka W, Zeng W, Tanen M, Wang AQ, Chen L, Winchell G, Davies MJ, Ramael S, Wagner JA, Herman GA.** Pharmacokinetic and pharmacodynamic properties of multiple oral doses of sitagliptin, a dipeptidyl peptidase-IV inhibitor: a double-blind, randomized, placebo-controlled study in healthy male volunteers. *Clin Ther* 28: 55–72, 2006.
5. **Bhashyam S, Fields AV, Patterson B, Testani JM, Chen L, Shen YT, Shannon RP.** Glucagon-like peptide-1 increases myocardial glucose uptake via p38alpha MAP kinase-mediated, nitric oxide-dependent mechanisms in conscious dogs with dilated cardiomyopathy. *Circ Heart Fail* 3: 512–521, 2010.
6. **Bose AK, Mocanu MM, Carr RD, Brand CL, Yellon DM.** Glucagon-like peptide 1 can directly protect the heart against ischemia/reperfusion injury. *Diabetes* 54: 146–151, 2005.
7. **Brandt I, Lambeir AM, Ketelslegers JM, Vanderheyden M, Scharpe S, De Meester I.** Dipeptidyl-peptidase IV converts intact B-type natriuretic peptide into its des-SerPro form. *Clin Chem* 52: 82–87, 2006.
8. **Bullock BP, Heller RS, Habener JF.** Tissue distribution of messenger ribonucleic acid encoding the rat glucagon-like peptide-1 receptor. *Endocrinology* 137: 2968–2978, 1996.
9. **Chaykovska L, von Websky K, Rahnenfuhrer J, Alter M, Heiden S, Fuchs H, Runge F, Klein T, Hocher B.** Effects of DPP-4 inhibitors on the heart in a rat model of uremic cardiomyopathy. *PloS One* 6: e27861, 2011.
10. **Cohn JN, Goldstein SO, Greenberg BH, Lorell BH, Bourge RC, Jaski BE, Gottlieb SO, McGrew F, 3rd DeMets DL, White BG.** A dose-dependent increase in mortality with vesnarinone among patients with severe heart failure. Vesnarinone Trial Investigators. *N Engl J Med* 339: 1810–1816, 1998.
11. **Deacon CF, Nauck MA, Toft-Nielsen M, Pridal L, Willms B, Holst JJ.** Both subcutaneously and intravenously administered glucagon-like peptide I are rapidly degraded from the NH2-terminus in type II diabetic patients and in healthy subjects. *Diabetes* 44: 1126–1131, 1995.
12. **Egstrup M, Kistorp CN, Schou M, Hofsten DE, Moller JE, Tuxen CD, Gustafsson I.** Abnormal glucose metabolism is associated with reduced left ventricular contractile reserve and exercise intolerance in patients with chronic heart failure. *Eur Heart J Cardiovasc Imaging* 14: 349–357, 2013.
13. **Falcao-Pires I, Hamdani N, Borbely A, Gavina C, Schalkwijk CG, van der Velden J, van Heerebeek L, Stienen GJ, Niessen HW, Leite-Moreira AF, Paulus WJ.** Diabetes mellitus worsens diastolic left ventricular dysfunction in aortic stenosis through altered myocardial structure and cardiomyocyte stiffness. *Circulation* 124: 1151–1159, 2011.
14. **Gomez N, Touihri K, Matheeussen V, Mendes Da Costa A, Mahmoudabady M, Mathieu M, Baerts L, Peace A, Lybaert P, Scharpe S, De Meester I, Bartunek J, Vanderheyden M, McEntee K.** Dipeptidyl peptidase IV inhibition improves cardiorenal function in overpacing-induced heart failure. *Eur J Heart Fail* 14: 14–21, 2012.
15. **Greig NH, Holloway HW, De Ore KA, Jani D, Wang Y, Zhou J, Garant MJ, Egan JM.** Once daily injection of exendin-4 to diabetic mice achieves long-term beneficial effects on blood glucose concentrations. *Diabetologia* 42: 45–50, 1999.
16. **Gutzwiller JP, Drewe J, Goke B, Schmidt H, Rohrer B, Lareida J, Beglinger C.** Glucagon-like peptide-1 promotes satiety and reduces food intake in patients with diabetes mellitus type 2. *Am J Physiol Regul Integr Comp Physiol* 276: R1541–R1544, 1999.
17. **Halbirk M, Norrelund H, Moller N, Holst JJ, Schmitz O, Nielsen R, Nielsen-Kudsk JE, Nielsen SS, Nielsen TT, Eiskjaer H, Botker HE, Wiggers H.** Cardiovascular and metabolic effects of 48-h glucagon-like peptide-1 infusion in compensated chronic patients with heart failure. *Am J Physiol Heart Circ Physiol* 298: H1096–H1102, 2010.
18. **Hui H, Farilla L, Merkel P, Perfetti R.** The short half-life of glucagon-like peptide-1 in plasma does not reflect its long-lasting beneficial effects. *Eur J Endocrinol* 146: 863–869, 2002.
19. **Hui H, Nourparvar A, Zhao X, Perfetti R.** Glucagon-like peptide-1 inhibits apoptosis of insulin-secreting cells via a cyclic 5′-adenosine monophosphate-dependent protein kinase A- and a phosphatidylinositol 3-kinase-dependent pathway. *Endocrinology* 144: 1444–1455, 2003.
20. **Kane GC, Karon BL, Mahoney DW, Redfield MM, Roger VL, Burnett JC Jr, Jacobsen SJ, Rodeheffer RJ.** Progression of left ventricular diastolic dysfunction and risk of heart failure. *JAMA* 306: 856–863, 2011.
21. **Kim J, Nakatani S, Hashimura K, Komamura K, Kanzaki H, Asakura M, Asanuma H, Kokubo Y, Tomoike H, Kitakaze M.** Abnormal glucose tolerance contributes to the progression of chronic heart failure in patients with dilated cardiomyopathy. *Hypertens Res* 29: 775–782, 2006.
22. **Lang RM, Bierig M, Devereux RB, Flachskampf FA, Foster E, Pellikka PA, Picard MH, Roman MJ, Seward J, Shanewise JS, Solomon SD, Spencer KT, Sutton MS, Stewart WJ.** Recommendations for chamber quantification: a report from the American Society of Echocardiography's Guidelines and Standards Committee and the Chamber Quantification Writing Group, developed in conjunction with the European Association of Echocardiography, a branch of the European Society of Cardiology. *J Am Soc Echocardiogr* 18: 1440–1463, 2005.
23. **Lenski M, Kazakov A, Marx N, Bohm M, Laufs U.** Effects of DPP-4 inhibition on cardiac metabolism and function in mice. *J Mol Cell Cardiol* 51: 906–918, 2011.
24. **Liao Y, Ishikura F, Beppu S, Asakura M, Takashima S, Asanuma H, Sanada S, Kim J, Ogita H, Kuzuya T, Node K, Kitakaze M, Hori M.** Echocardiographic assessment of LV hypertrophy and function in aortic-banded mice: necropsy validation. *Am J Physiol Heart Circ Physiol* 282: H1703–H1708, 2002.
25. **Liao Y, Takashima S, Asano Y, Asakura M, Ogai A, Shintani Y, Minamino T, Asanuma H, Sanada S, Kim J, Ogita H, Tomoike H, Hori M, Kitakaze M.** Activation of adenosine A1 receptor attenuates cardiac hypertrophy and prevents heart failure in murine left ventricular pressure-overload model. *Circ Res* 93: 759–766, 2003.
26. **Liao Y, Takashima S, Maeda N, Ouchi N, Komamura K, Shimomura I, Hori M, Matsuzawa Y, Funahashi T, Kitakaze M.** Exacerbation of heart failure in adiponectin-deficient mice due to impaired regulation of AMPK and glucose metabolism. *Cardiovasc Res* 67: 705–713, 2005.
27. **Liao Y, Takashima S, Zhao H, Asano Y, Shintani Y, Minamino T, Kim J, Fujita M, Hori M, Kitakaze M.** Control of plasma glucose with alpha-glucosidase inhibitor attenuates oxidative stress and slows the progression of heart failure in mice. *Cardiovasc Res* 70: 107–116, 2006.
28. **Lind M, Bounias I, Olsson M, Gudbjornsdottir S, Svensson AM, Rosengren A.** Glycaemic control and incidence of heart failure in 20,985 patients with type 1 diabetes: an observational study. *Lancet* 378: 140–146, 2011.
29. **Livak KJ, Schmittgen TD.** Analysis of relative gene expression data using real-time quantitative PCR and the 2[−Delta Delta C(T)] method. *Methods* 25: 402–408, 2001.
30. **Lucas JA, Zhang Y, Li P, Gong K, Miller AP, Hassan E, Hage F, Xing D, Wells B, Oparil S, Chen YF.** Inhibition of transforming growth factor-beta signaling induces left ventricular dilation and dysfunction in the pressure-overloaded heart. *Am J Physiol Heart Circ Physiol* 298: H424–H432, 2010.
31. **Mariappan N, Elks CM, Sriramula S, Guggilam A, Liu Z, Borkhsenious O, Francis J.** NF-kappaB-induced oxidative stress contributes to mitochondrial and cardiac dysfunction in type II diabetes. *Cardiovasc Res* 85: 473–483, 2010.
32. **Mentlein R, Dahms P, Grandt D, Kruger R.** Proteolytic processing of neuropeptide Y and peptide YY by dipeptidyl peptidase IV. *Regul Pept* 49: 133–144, 1993.
33. **Nikolaidis LA, Doverspike A, Hentosz T, Zourelias L, Shen YT, Elahi D, Shannon RP.** Glucagon-like peptide-1 limits myocardial stunning following brief coronary occlusion and reperfusion in conscious canines. *J Pharmacol Exper Ther* 312: 303–308, 2005.
34. **Nikolaidis LA, Elahi D, Hentosz T, Doverspike A, Huerbin R, Zourelias L, Stolarski C, Shen YT, Shannon RP.** Recombinant glucagon-like peptide-1 increases myocardial glucose uptake and improves left ventricular performance in conscious dogs with pacing-induced dilated cardiomyopathy. *Circulation* 110: 955–961, 2004.

35. **Okada K, Minamino T, Tsukamoto Y, Liao Y, Tsukamoto O, Takashima S, Hirata A, Fujita M, Nagamachi Y, Nakatani T, Yutani C, Ozawa K, Ogawa S, Tomoike H, Hori M, Kitakaze M.** Prolonged endoplasmic reticulum stress in hypertrophic and failing heart after aortic constriction: possible contribution of endoplasmic reticulum stress to cardiac myocyte apoptosis. *Circulation* 110: 705–712, 2004.
36. **Paolisso G, Tagliamonte MR, Rizzo MR, Gambardella A, Gualdiero P, Lama D, Varricchio G, Gentile S, Varricchio M.** Prognostic importance of insulin-mediated glucose uptake in aged patients with congestive heart failure secondary to mitral and/or aortic valve disease. *Am J Cardiol* 83: 1338–1344, 1999.
37. **Redfield MM, Jacobsen SJ, Burnett JC Jr, Mahoney DW, Bailey KR, Rodeheffer RJ.** Burden of systolic and diastolic ventricular dysfunction in the community: appreciating the scope of the heart failure epidemic. *JAMA* 289: 194–202, 2003.
38. **Rijzewijk LJ, van der Meer RW, Lamb HJ, de Jong HW, Lubberink M, Romijn JA, Bax JJ, de Roos A, Twisk JW, Heine RJ, Lammertsma AA, Smit JW, Diamant M.** Altered myocardial substrate metabolism and decreased diastolic function in nonischemic human diabetic cardiomyopathy: studies with cardiac positron emission tomography and magnetic resonance imaging. *J Am Coll Cardiol* 54: 1524–1532, 2009.
39. **Roy S, Khanna V, Mittra S, Dhar A, Singh S, Mahajan DC, Priyadarsiny P, Davis JA, Sattigeri J, Saini KS, Bansal VS.** Combination of dipeptidylpeptidase IV inhibitor and low dose thiazolidinedione: preclinical efficacy and safety in *db/db* mice. *Life Sci* 81: 72–79, 2007.
40. **Sanada S, Kitakaze M, Papst PJ, Asanuma H, Node K, Takashima S, Asakura M, Ogita H, Liao Y, Sakata Y, Ogai A, Fukushima T, Yamada J, Shinozaki Y, Kuzuya T, Mori H, Terada N, Hori M.** Cardioprotective effect afforded by transient exposure to phosphodiesterase III inhibitors: the role of protein kinase A and p38 mitogen-activated protein kinase. *Circulation* 104: 705–710, 2001.
41. **Sasaki H, Asanuma H, Fujita M, Takahama H, Wakeno M, Ito S, Ogai A, Asakura M, Kim J, Minamino T, Takashima S, Sanada S, Sugimachi M, Komamura K, Mochizuki N, Kitakaze M.** Metformin prevents progression of heart failure in dogs: role of AMP-activated protein kinase. *Circulation* 119: 2568–2577, 2009.
42. **Sauve M, Ban K, Momen MA, Zhou YQ, Henkelman RM, Husain M, Drucker DJ.** Genetic deletion or pharmacological inhibition of dipeptidyl peptidase-4 improves cardiovascular outcomes after myocardial infarction in mice. *Diabetes* 59: 1063–1073, 2010.
43. **Savage DB, Petersen KF, Shulman GI.** Mechanisms of insulin resistance in humans and possible links with inflammation. *Hypertension* 45: 828–833, 2005.
44. **Schweizer A, Dejager S, Foley JE, Couturier A, Ligueros-Saylan M, Kothny W.** Assessing the cardio-cerebrovascular safety of vildagliptin: meta-analysis of adjudicated events from a large Phase III type 2 diabetes population. *Diabetes Obesity Metab* 12: 485–494, 2010.
45. **Shigeta T, Aoyama M, Bando YK, Monji A, Mitsui T, Takatsu M, Cheng XW, Okumura T, Hirashiki A, Nagata K, Murohara T.** Dipeptidyl peptidase-4 modulates left ventricular dysfunction in chronic heart failure via angiogenesis-dependent and -independent actions. *Circulation* 126: 1838–1851, 2012.
46. **Shimizu I, Minamino T, Toko H, Okada S, Ikeda H, Yasuda N, Tateno K, Moriya J, Yokoyama M, Nojima A, Koh GY, Akazawa H, Shiojima I, Kahn CR, Abel ED, Komuro I.** Excessive cardiac insulin signaling exacerbates systolic dysfunction induced by pressure overload in rodents. *J Clin Invest* 120: 1506–1514, 2010.
47. **Shioda T, Kato H, Ohnishi Y, Tashiro K, Ikegawa M, Nakayama EE, Hu H, Kato A, Sakai Y, Liu H, Honjo T, Nomoto A, Iwamoto A, Morimoto C, Nagai Y.** Anti-HIV-1 and chemotactic activities of human stromal cell-derived factor 1alpha (SDF-1alpha) and SDF-1beta are abolished by CD26/dipeptidyl peptidase IV-mediated cleavage. *Proc Natl Acad Sci USA* 95: 6331–6336, 1998.
48. **Sokos GG, Nikolaidis LA, Mankad S, Elahi D, Shannon RP.** Glucagon-like peptide-1 infusion improves left ventricular ejection fraction and functional status in patients with chronic heart failure. *J Card Fail* 12: 694–699, 2006.
49. **Stolen KQ, Kemppainen J, Kalliokoski KK, Luotolahti M, Viljanen T, Nuutila P, Knuuti J.** Exercise training improves insulin-stimulated myocardial glucose uptake in patients with dilated cardiomyopathy. *J Nucl Cardiol* 10: 447–455, 2003.
50. **Suskin N, McKelvie RS, Burns RJ, Latini R, Pericak D, Probstfield J, Rouleau JL, Sigouin C, Solymoss CB, Tsuyuki R, White M, Yusuf S.** Glucose and insulin abnormalities relate to functional capacity in patients with congestive heart failure. *Eur Heart J* 21: 1368–1375, 2000.
51. **Swan JW, Anker SD, Walton C, Godsland IF, Clark AL, Leyva F, Stevenson JC, Coats AJ.** Insulin resistance in chronic heart failure: relation to severity and etiology of heart failure. *J Am Coll Cardiol* 30: 527–532, 1997.
52. **Szeto IM, Aziz A, Das PJ, Taha AY, Okubo N, Reza-Lopez S, Giacca A, Anderson GH.** High multivitamin intake by Wistar rats during pregnancy results in increased food intake and components of the metabolic syndrome in male offspring. *Am J Physiol Regul Integr Comp Physiol* 295: R575–R582, 2008.
53. **Thrainsdottir IS, Aspelund T, Thorgeirsson G, Gudnason V, Hardarson T, Malmberg K, Sigurdsson G, Ryden L.** The association between glucose abnormalities and heart failure in the population-based Reykjavik study. *Diabetes Care* 28: 612–616, 2005.
54. **Toye AA, Lippiat JD, Proks P, Shimomura K, Bentley L, Hugill A, Mijat V, Goldsworthy M, Moir L, Haynes A, Quarterman J, Freeman HC, Ashcroft FM, Cox RD.** A genetic and physiological study of impaired glucose homeostasis control in C57BL/6J mice. *Diabetologia* 48: 675–686, 2005.
55. **Trevaskis JL, Griffin PS, Wittmer C, Neuschwander-Tetri BA, Brunt EM, Dolman CS, Erickson MR, Napora J, Parkes DG, Roth JD.** Glucagon-like peptide-1 receptor agonism improves metabolic, biochemical, and histopathological indices of nonalcoholic steatohepatitis in mice. *Am J Physiol Gastrointest Liver Physiol* 302: G762–G772, 2012.
56. **Vasan RS, Larson MG, Benjamin EJ, Evans JC, Reiss CK, Levy D.** Congestive heart failure in subjects with normal versus reduced left ventricular ejection fraction: prevalence and mortality in a population-based cohort. *J Am Coll Cardiol* 33: 1948–1955, 1999.
57. **Wei Y, Mojsov S.** Tissue-specific expression of the human receptor for glucagon-like peptide-I: brain, heart and pancreatic forms have the same deduced amino acid sequences. *FEBS Lett* 358: 219–224, 1995.
58. **Winzell MS, Ahren B.** The high-fat diet-fed mouse: a model for studying mechanisms and treatment of impaired glucose tolerance and type 2 diabetes. *Diabetes* 53, *Suppl* 3: S215–S219, 2004.
59. **Ye Y, Keyes KT, Zhang C, Perez-Polo JR, Lin Y, Birnbaum Y.** The myocardial infarct size-limiting effect of sitagliptin is PKA-dependent, whereas the protective effect of pioglitazone is partially dependent on PKA. *Am J Physiol Heart Circ Physiol* 298: H1454–H1465, 2010.
60. **Yin M, Sillje HH, Meissner M, van Gilst WH, de Boer RA.** Early and late effects of the DPP-4 inhibitor vildagliptin in a rat model of post-myocardial infarction heart failure. *Cardiovasc Diabetol* 10: 85, 2011.

Cardiovasc Drugs Ther (2012) 26:217–226
DOI 10.1007/s10557-012-6381-5

H_2 Mediates Cardioprotection Via Involvements of K_{ATP} Channels and Permeability Transition Pores of Mitochondria in Dogs

Akemi Yoshida · Hiroshi Asanuma · Hideyuki Sasaki · Shoji Sanada · Satoru Yamazaki · Yoshihiro Asano · Yoshiro Shinozaki · Hidezo Mori · Akito Shimouchi · Motoaki Sano · Masanori Asakura · Tetsuo Minamino · Seiji Takashima · Masaru Sugimachi · Naoki Mochizuki · Masafumi Kitakaze

Published online: 17 April 2012

Abstract
Purpose Inhalation of hydrogen (H_2) gas has been shown to limit infarct size following ischemia-reperfusion injury in rat hearts. However, H_2 gas-induced cardioprotection has not been tested in large animals and the precise cellular mechanism of protection has not been elucidated. We investigated whether opening of mitochondrial ATP-sensitive K+ channels (mK_{ATP}) and subsequent inhibition of mitochondrial permeability transition pores (mPTP) mediates the infarct size-limiting effect of H_2 gas in canine hearts.
Methods The left anterior descending coronary artery of beagle dogs was occluded for 90 min followed by reperfusion for 6 h. Either 1.3% H_2 or control gas was inhaled from 10 min prior to start of reperfusion until 1 h of reperfusion, in the presence or absence of either 5-hydroxydecanoate (5-HD; a selective mK_{ATP} blocker), or atractyloside (Atr, a mPTP opener).
Results Systemic hemodynamic parameters did not differ among the groups. Nevertheless, H_2 gas inhalation reduced infarct size normalized by risk area (20.6±2.8% vs. control gas 44.0±2.0%; $p<0.001$), and administration of either 5-HD or Atr abolished the infarct size-limiting effect of H_2 gas (42.0±2.2% with 5-HD and 45.1±2.7% with Atr; both $p<0.001$ vs. H_2 group). Neither Atr nor 5-HD affected infarct size per se. Among all groups, NAD content and the number of apoptotic and 8-OHdG positive cells was not significantly different, indicating that the cardioprotection

A. Yoshida · H. Sasaki · S. Yamazaki · M. Asakura · M. Kitakaze (✉)
Department of Cardiovascular Medicine, National Cerebral and Cardiovascular Center, Suita 565-8565, Osaka, Japan
e-mail: kitakaze@zf6.so-net.ne.jp

H. Asanuma
Department of Cardiovascular Science and Technology, Kyoto Prefectural University of Medicine, Suita 565-8565, Osaka, Japan

A. Yoshida · N. Mochizuki
Department of Structural Analysis, National Cerebral and Cardiovascular Research Center, Suita, Japan

S. Sanada · Y. Asano · T. Minamino · S. Takashima
Department of Cardiovascular Medicine, Osaka University Graduate School of Medicine, Suita, Japan

Y. Shinozaki · H. Mori
Department of Physiological Science, Tokai University Graduate School of Medicine, Isehara, Japan

A. Shimouchi
Department of Cardiac Physiology, National Cerebral and Cardiovascular Research Center, Suita, Japan

M. Sano
Department of Cardiology, Keio University School of Medicine, Tokyo, Japan

M. Sugimachi
Department of Cardiovascular Dynamics, Research Institute, National Cerebral and Cardiovascular Center, Suita, Japan

afforded by H_2 was not due to anti-oxidative actions or effects on the NADH dehydrogenase pathway.
Conclusions Inhalation of H_2 gas reduces infarct size in canine hearts via opening of mitochondrial K_{ATP} channels followed by inhibition of mPTP. H_2 gas may provide an effective adjunct strategy in patients with acute myocardial infarction receiving reperfusion therapy.

Key words Hydrogen gas · Reperfusion injury · Myocardial infarction · Mitochondrial K_{ATP} channel · Mitochondrial permeability transition pore

Introduction

Myocardial infarction (MI) is a leading cause of death worldwide, and reduction of infarct size is an important therapeutic goal for patients with acute MI (AMI). The prognosis of AMI has been improved dramatically due to the development of both catheterization techniques and reperfusion therapy by coronary mechanical methods or pharmacological intervention. However, strategies to limit reperfusion injury and thus infarct size have not been well applied in clinical settings [1, 2]. We reported that carperitide limited infarct size in a large scale clinical trial [3]; however, infarct size was reduced by only 14.7%, and the discovery of other therapeutics to limit infarct size may be clinically useful. Interestingly, hydrogen (H_2) has been reported to provide therapeutic benefit for many diseases related to oxidative stress, including cardiovascular disease. There is some evidence that inhalation of H_2 gas limits myocardial infarct size in rats [4, 5]. However, since heart physiology differs significantly in small animals relative to large animals and humans, it cannot be assumed that H_2 would limit infarct size in large animals and humans. Furthermore, the cellular mechanisms underlying H_2-mediated cardioprotection have not been clarified.

Recent accumulated evidence regarding cardioprotection afforded by ischemic pre- or post-conditioning has culminated in the idea that opening of mitochondrial ATP-sensitive K^+ channels (mK_{ATP}) followed by inhibition of mitochondrial permeability transition pores (mPTP) plays a central role in limiting infarct size [6–8]. Indeed, Piot et al. [9] found that administration of the mPTP inhibitor, cyclosporine, at the time of reperfusion limited the size of myocardial infarction in patients with AMI. Ohsawa et al. [10] demonstrated that H_2 has the potential to serve as an antioxidant in preventive and therapeutic applications. Oxygen-derived free radicals are generated inside and outside of cells, and H_2 gas can eliminate hydoxyradical and peroxynitrate because it can penetrate biomembranes and diffuse into the cytosol, mitochondria, and nuclei. If this is the case, H_2 gas may protect mK_{ATP} against ischemic injury, or may directly activate mK_{ATP} followed by the inhibition of mPTP.

Thus, we tested the hypothesis that H_2 gas may reduce reperfusion injury and limit infarct size via the activation of mK_{ATP} and the inhibition of mPTP.

Methods

Animal model and instrumentation

Fifty nine beagle dogs (Oriental Yeast Co., Ltd, Tokyo, Japan) weighing 9 to 10 kg were per-anesthetized with sodium pentobarbital (25 mg/kg iv). All dogs were rapidly intubated and anesthetized with analgesic anesthetics. The control or H_2 gas tank was connected to the respirator 10 min before reperfusion. After baseline hemodynamic assessment, thoracotomy was performed, and the left anterior descending coronary artery (LAD) was ligated just distal to the first diagonal branch. The left carotid artery was catheterized to monitor both aortic blood pressure and heart rate. At the end of each study, animals were euthanized with administration of a high dose of sodium pentobarbital. All procedures were performed in conformity with the Guide for the Care and Use of Laboratory Animals (NIH publication no. 85-23, 1996 revision).

Composition of gas mixture

Gas tanks were obtained from TAIYO NIPPON SANSO Corporation (Osaka, Japan). The control gas tanks were composed of 70% N_2 and 30% O_2. The H_2 gas tanks were composed of 1.3% H_2, 68.7% N_2, and 30% O_2. The H_2 gas concentration was set at 1.3% because higher concentrations create the possibility of explosion. Previous studies showed that 0.5%–4.0% H_2 limited infarct size in rat hearts in vivo, at a flow rate of 1 L/min.

Experimental protocols

After the randomization to either H_2 gas (n=18) or control gas (n=18), the LAD of the beagle was occluded for 90 min followed by reperfusion for 6 h. Either H_2 gas or control gas was inhaled (3.36 L/min) 10 min prior to reperfusion until 1 h of reperfusion. In addition, we intravenously administered either 5-hydroxydecanoate (5-HD, Sigma; 10 mg/kg i.v.), or atractyloside (Atr, Sigma; 2.5 mg/kg i.v.), for 5 min before gas inhalation [H_2 gas with 5-HD (n=6) or Atr (n=6) and control gas with 5-HD (n=6) or Atr (n=6)]. In all groups, infarct size was assessed after 6 h of reperfusion. We also investigated apoptosis in the myocardium adjacent to the infarct area using TUNEL staining. In addition, we counted the incidence of lethal arrhythmia, defined as more than 15 consecutive premature ventricular contractions (VPC) or ventricular fibrillation (Vf) from 10 min before reperfusion to 60 min after the onset of reperfusion.

Measurement of infarct size and myocardial collateral blood flow

We measured both area at risk and infarct area 6 h after the onset of reperfusion as described previously [11]. These parameters were evaluated by Evans blue and triphenyltetrazolium chloride (TTC) staining, respectively. Infarct size was calculated as [infarct area/area at risk] × 100(%).

Regional myocardial blood flow was determined by the microsphere technique. Non-radioactive microspheres (Sekisui Plastic Co., Ltd., Tokyo, Japan) are made of inert plastic labeled with niobium (Nb) and bromine (Br) as described in detail in previous study [12]. Microspheres were suspended in isotonic saline with 0.01% Tween80 to prevent aggregation. The microspheres were ultrasonicated for 5 min followed by 5 min of vortexing immediately before injection. Approximately 1 mL of the microsphere suspension ($2–4\times10^5$ spheres) was injected into the left atrium at 80 min after the start of coronary occlusion.

The X-ray fluorescence of stable heavy elements was measured by a wavelength dispersive spectrometer (PW 1480, PHILLIPS Co., Ltd.). The specifications of this X-ray fluorescence spectrometer have been described previously [12]. In brief, when the microspheres are irradiated by the primary X-ray beam, the electrons fall back to a lower orbit and emit measurable energy. The energy level of the X-ray fluorescence depends on the characteristics of each element. Therefore, it was possible to quantify the X-ray fluorescence of several differently labeled microspheres in the mixture. Regional myocardial collateral blood flow was calculated according to the following formula: time flow = (tissue count) × (reference flow)/(reference count), and was expressed in mL/g wet weight/min.

Terminal Deoxynucleotidyl transferase-mediated dUTP nick-end labeling (TUNEL)

The myocardial tissue samples were taken from the border zone of dogs in the control, H_2, control+5-HD, H_2+5-HD, control+Atr and H_2+Atr groups (n=3 each). The border zone was chosen as the region within 4 mm from the infarct zone. These were fixed in 10% buffered formalin, embedded in paraffin, and serially sectioned in the frontal plane at 5-μm thickness. To assess myocardial apoptosis, analysis by TUNEL method was performed according to the protocol supplied with the in situ apoptosis detection kit, the Apop Tag Peroxidase In Situ Apoptosis Detection Kit (S7100, MILLIPORE). The sections were then shortly counterstained with hematoxylin and eosin to visualize the cells. TUNEL-positive cell nuclei and total cell nuclei stained metylgreen were counted in 7–10 random high-power fields (×200). The amount of TUNEL-positive cells was expressed as a percentage of the total amount of cells (n=1,500).

Immunohistochemistry for either 8-OHdG or NAD+ of the Reperfused myocardium

The myocardial tissue samples were taken from the border zone between ischemic and non-ischemic areas in the control, H_2, H_2+5-HD, H_2+Atr, control+5-HD and control+Atr groups (n=3 each). After 90 min of ischemia followed by 6 h of reperfusion, hearts were excised and the myocardial tissue samples were taken from the border zone. The border zone was chosen as the region within 4 mm from the infarct zone. These were fixed in 10% buffered formalin, embedded in paraffin, and serially sectioned in the frontal plane at 5-μm thickness. The paraffin sections were deparaffinized in xylene, rehydrated using various grades of ethanol, and pretreated with 10 mM citric acid for 40 min at 95°C. For immunostaining, sections stained with anti-8OH-dG (MOG-020P; Japan Institute for the Control of Aging; 1:100) antibodies overnight at 4°C. Secondary antibodies conjugated Simple Stain Rat (MAX-PO MULTI 414191, NICHIREI Bioscience inc. Japan; undiluted) were applied for 30 min at room temperature. The sections were then shortly counterstained with hematoxylin and eosin to visualize the cells. Four slides were randomly examined using a defined rectangular field area with magnification (×40). The data were represented as the number of 8OH-dG positive cells per field.

Since mPTP may be opened via oygen-drived free radicals via the NADPH oxidase, we also investigated the myocardial NAD+ contents as well. We used 18 dogs for NAD assessment in the control, H_2, H_2+5-HD, H_2+Atr, control+5-HD and control+Atr groups (n=3 each). The myocardial tissue in the border zone was quickly placed into liquid nitrogen and stored at −80°C. For the measurement of NAD+, 40 mg of border zone tissue was homogenized. An equal amount of protein from the homogenized tissue of each group was used for the NAD+/NADH Colorimetric assay kit (Cat# CY-1253; Cyclex Co., Ltd).

Exclusion criteria

To ensure that all animals used in the present study were healthy and had been exposed to a similar extent of ischemia, the following standards were employed for the exclusion of unsatisfactory dogs: (1) subendocardial collateral blood flow greater than 15 mL/100 g/min; (2) heart rate greater than 170 beats/min; and (3) more than two consecutive attempts required to terminate ventricular fibrillation (Vf) using low-energy DC pulses applied directly to the heart.

Statistical analysis

Statistical analysis was performed using two-way repeated measures analysis of variance (ANOVA) when data were

compared over the time course of the change between groups. Analysis of covariance between regional collateral flow in the inner half of the left ventricular wall and infarct size was described previously [11]. Other data were compared using one-way fractional analysis of variance. If statistical significance was found for a group, time effect, or group-by-time interaction, further comparisons were made with paired *t* tests between all possible pairs of the five groups at individual time points. Results were expressed as means ± SEM, with $p<0.05$ considered statistically significant.

Results

Among the 59 dogs, 23 were excluded due to Vf or excessive myocardial collateral blood flow (>15 mL/100 g/min). The remaining 36 dogs completed the protocols satisfactorily and were included in the data analysis. None of the pharmacological interventions such as H_2 gas, control gas, 5-HD, or Atr, altered systemic blood pressure or heart rate during the experimental protocols (Table 1).

Inhalation of H_2 gas just prior to reperfusion following 90 min of ischemia reduced infarct size normalized by risk area (20.6±2.8% vs. 44.0±2.0%; $p<0.001$) (Fig. 1). Intriguingly, the administration of either 5-HD or atractyloside (Atr) blunted the H_2 gas induced limiting effect on infarct size (42.0 ±2.2% in 5-HD vs. 45.1±2.7% in Atr; $p<0.001$ and $p<0.001$ vs. H_2 gas group). Neither 5-HD nor atractyloside per se affected infarct size. There were no differences in either risk area or collateral flow during the ischemic period among the groups (Fig. 2). Figure 3 shows the regression plots of the area at risk vs. collateral flow. Inhalation of H_2 gas mediated the substantial cardioprotection irrespective of collateral flow, which was again blunted by either 5-HD or atractyloside.

On the other hand, we observed apoptosis using TUNEL staining in the myocardium in each group; there were no differences in the extent of apoptosis in the groups (36.0± 1.8, 26.5±6.9, 33.0±1.4, 35.6±1.5, 35.0±1.3 and 35.7±1.4% in the control group, the H_2 gas group, the H_2 gas with 5HD group, the H_2 gas with Atr group, the control gas with 5HD group, and the control gas with Atr group, respectively).

We observed the incidence of lethal arrhythmia throughout the experiments in all groups from 10 min before reperfusion to 60 min after the onset of reperfusion (Table 2). The presence of either Vf or VPC longer than 15 consecutive beats was defined as lethal arrhythmia in this study. The incidence of lethal arrhythmia in the reperfusion period tended to decrease by H_2 gas although there were no significant differences. This tendency was blunted by either 5-HD or Atr. These data indicate that H_2 gas may affect the incidence of fatal ventricular arrhythmias during the reperfusion period, but it is unknown whether this effect is attributable to a potential primary anti-arrhythmic effect of H_2 gas or merely secondary to the infarct size-limiting effects of H_2 gas.

The number of 8-OHdG (a biomarker of oxidative stress) positive cells, tended to decrease in H_2 group relative to the other groups, however there was no significant difference (Fig. 4). We also observed no relation between the number

Table 1 Effect of H_2 gas on systemic hemodynamic parameters

Groups	Baseline	Isc-60	Isc-90	Rep-60	Rep-120	Rep-180	Rep-240	Rep-300	Rep-240
Mean blood pressure (mmHg)									
Control gas	101±2	103±2	104±2	98±2	102±2	101±3	103±3	99±3	100±2
H_2 gas	105±4	97±2	98±3	96±3	100±2	101±3	99±2	101±2	103±1
H_2 gas + 5HD	105±2	105±2	106±1	95±3	98±3	101±3	103±1	102±0	100±4
H_2 gas + Atr	98±3	98±3	102±3	98±1	100±1	101±1	102±1	102±2	103±1
Control gas + 5HD	104±2	101±2	101±1	102±2	103±2	101±3	103±2	98±3	100±4
Control gas + Atr	102±1	102±4	100±2	96±1	103±2	100±3	103±2	104±2	102±1
Heart rate (beats/min)									
Control gas	136±3	138±2	137±2	132±2	131±1	135±3	135±4	133±4	133±4
H_2 gas	139±3	138±3	140±4	133±3	134±4	134±5	134±4	134±5	132±4
H_2 gas + 5HD	135±3	130±3	129±4	129±3	129±4	130±3	129±4	129±4	130±3
H_2 gas + Atr	134±2	135±4	130±4	129±3	129±2	129±3	129±2	128±3	129±3
Control gas + 5HD	134±4	135±3	135±3	135±2	129±3	131±5	132±5	130±5	129±5
Control gas + Atr	137±2	137±2	135±3	136±2	137±3	135±4	135±2	135±3	136±2

Values are expressed as mean ± SEM. Isc-60 and Isc-90 show 60 and 90 min after the onset of myocardial ischemia, respectively. Rep-60, Rep-120, Rep-180, Rep-240, Rep-300 and Rep-360 show 60, 120, 180, 240, 300 and 360 min after the onset of reperfusion, respectively. There were no significant changes of theses parameters among the six groups

5HD = 5-hydroxydecanoate; Atr = Atractyloside

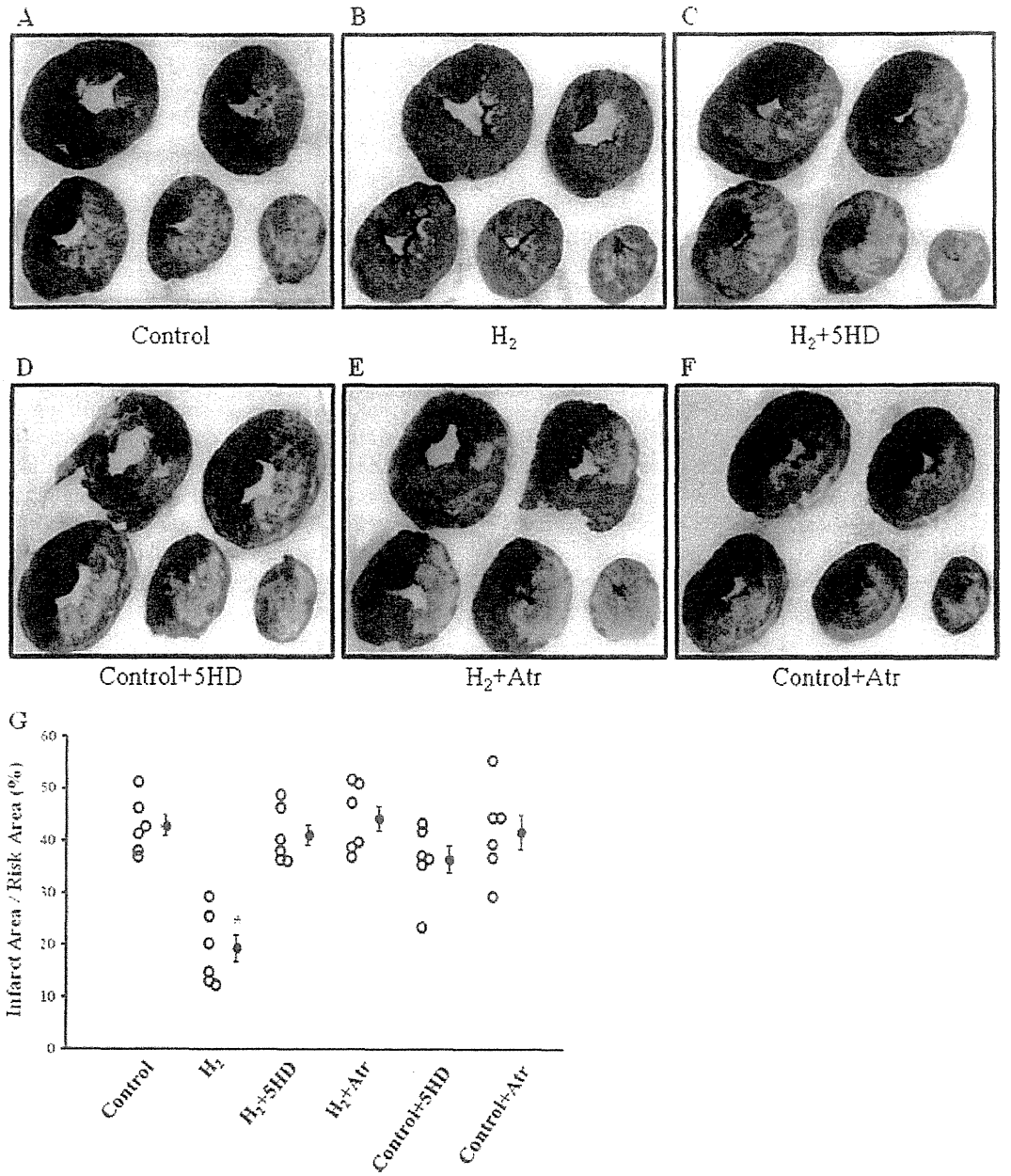

Fig. 1 Effect of H_2 Gas on Myocardial Infarct Size. Values are expressed as mean ± SEM (error bars). Representative photos following both Evans Blue and triphenyltetrazolium chloride staining are shown in the control gas (**A**), H_2 gas (**B**), H_2 gas with 5HD (**C**), H_2 gas with Atr (**D**), control gas with 5HD (**E**), and the control gas with Atr groups (**F**) respectively. G Myocardial infarct size quantification as a percentage of the area at risk in groups tested. Inhalation of hydrogen gas reduced infarct size. 5HD and Atr abolished this cardioprotective effect. *$p<0.0001$ vs. control group. 5HD = 5-hydroxydecanoate; Atr = atractyloside

of 8-OHdG positive cells and infarct size. We next investigated myocardial NAD+ levels and observed a not significant tendency towards increased NAD+ levels in the H_2 group, suggesting that the inhibition of mPTP caused by the opening of mK_{ATP} may not be attributable to oxygen-derived free radicals produced through NADH dehydrogenase (Fig. 5).

Discussion

The present study provides a novel finding that inhalation of H_2 gas mediates infarct size-limiting effects but not cellular apoptosis-limiting effects in the canine heart large animal model, and that H_2 gas-mediated cardioprotection is mainly attributable to the opening of mK_{ATP} followed by inhibition

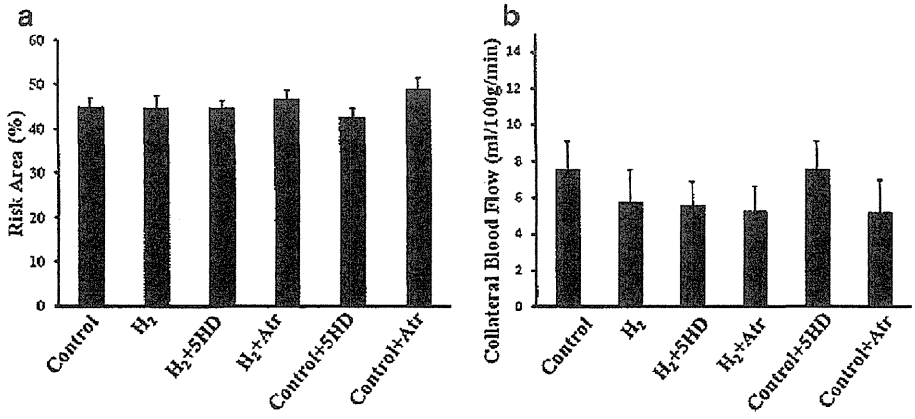

Fig. 2 Risk Area and Collateral Flow. Risk area (a) and collateral blood flow (b). There were no differences in either risk area or collateral blood flow in all groups. Values are expressed as mean ± SEM (error bars)

of mPTP, although we could not completely exclude the involvements of H_2 gas-mediated anti-oxidant effects on the present results.

Factors that affect infarct size during inhalation of H_2 gas

The infarct size-limiting effect of H_2 gas may be attributable to changes in systemic hemodynamics and/or collateral flow, because these two factors are critical in determining infarct size. However, when H_2 gas was inhaled, systemic blood pressure, heart rate, and collateral flow were unchanged among the groups. Therefore, H_2 gas-induced cardioprotection is not mediated by hemodynamic or collateral flow changes secondary to the inhalation of H_2 gas. Myocardial contractility is another determinant of infarct size, since increases in myocardial contractility may increase infarct size; indeed, beta blockers, which reduce myocardial contractility, reduce infarct size. However, Hayashida et al. [5] and Sun et al. [4] showed that either H_2 gas or H_2-rich saline provokes no changes in myocardial contractility as a index of maximal dP/dt, suggesting that myocardial contractility is not altered by H_2 gas, although we did not measure myocardial contractility in the present study.

We have shown that H_2 gas limits infarct size in large animals, which may be translated to human use. In rats, heart rate and maximal dP/dt are around 400/min, and 8,000 mmHg/sec, respectively [5]. However, in the anesthetized dog, these parameters are around 130/min and 4,000 mmHg/sec, respectively [13, 14]. Therefore, the fact that H_2 gas limits infarct size in rat hearts does not necessarily indicate that this will be the case in large animals. We found cardioprotective effects of H_2 gas in canine hearts, indicating that potent cardioprotection by H_2 gas or H_2-rich saline may be the case for possible human use. However, in our large animal model, apoptosis was not prevented by H_2 gas, which is different from results seen by Sun et al. [4]. We

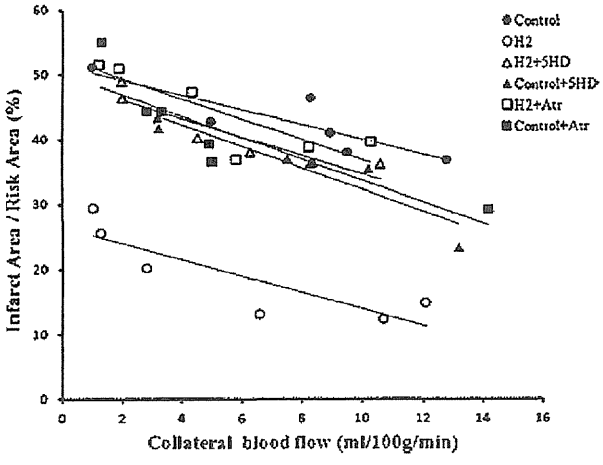

Fig. 3 Plot of infarct size expressed as a percentage of the risk area and regional collateral flow during ischemia. The abbreviations are same as in Fig. 1 There are inverse relations between normalized infarct area and collateral flow, and a significant difference ($P<0.05$) is seen in the H_2 gas group compared with the control group

Table 2 Incidence of lethal arrhythmia during ischemia and reperfusion periods and number of dogs excluded for lethal arrhythmia

Groups	Lethal arrhythmia		No. of excluded dogs	
	Ischemia period (counts)	Reperfusion period (counts)	Vf (counts)	Collateral blood flow (ml/100 g/min)
Control gas	0	23	1	3
H_2 gas	0	5	0	2
H_2 gas + 5HD	0	29	1	3
H_2 gas + Atr	0	27	1	3
Control gas + 5HD	0	28	2	2
Control gas + Atr	1	30	3	2

Incidence of lethal arrhythmia is shown in the included dogs of the present study. H_2 gas group tended to reduce incidence of lethal arrhythmia, however, there were no significant differences among the six groups. Vf = ventricular fibrillation; Abbreviations as in Table 1

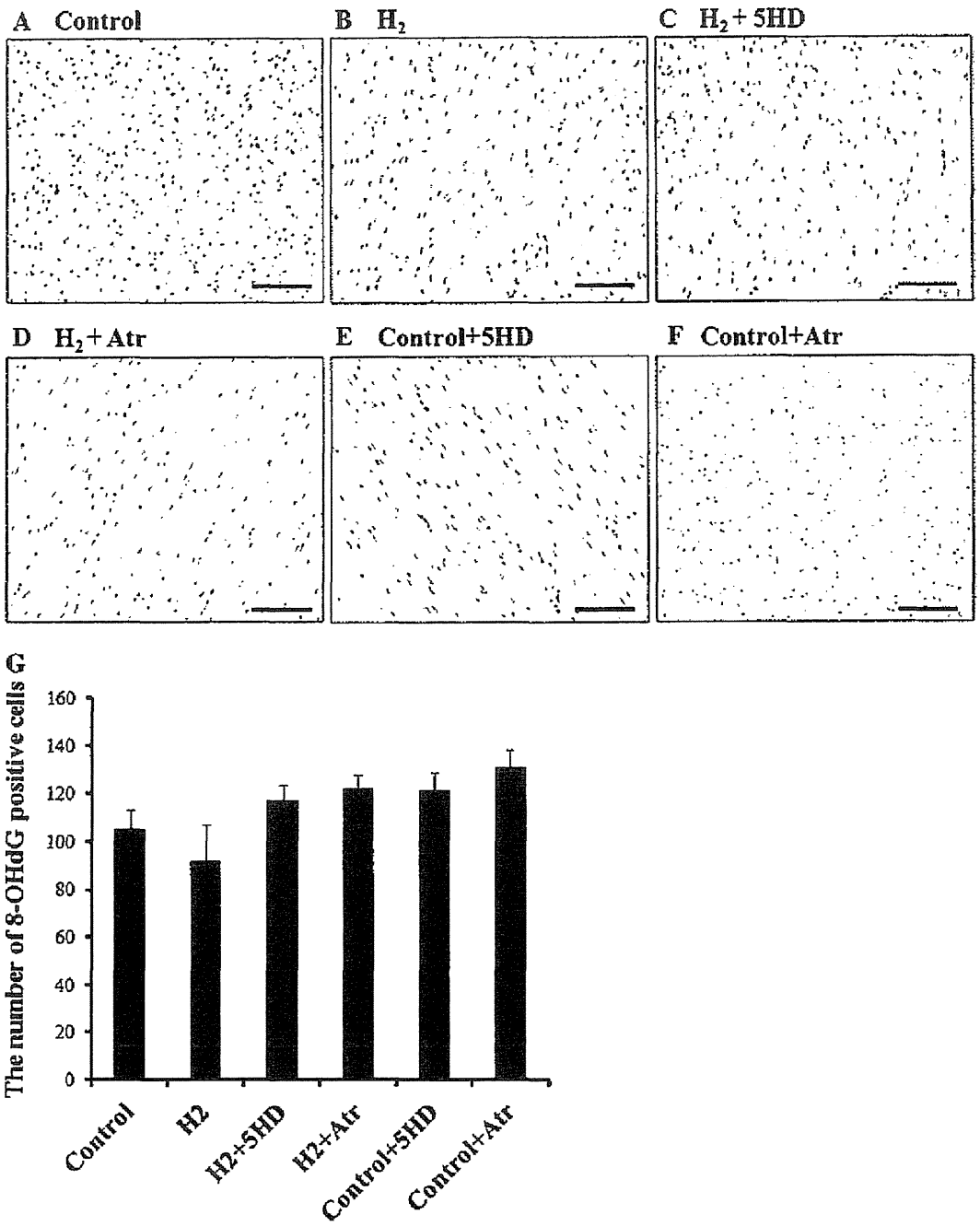

Fig. 4 The number of 8-OHdG positive cells. Representative photos assessed by 8-OHdG immunoreactivity. Staining was localized to nuclei of myocardium (brown) in the control gas (A), H_2 gas (B), H_2 gas with 5HD (C), H_2 gas with Atr (D), control gas with 5HD (E), and the control gas with Atr groups (F) respectively. Scale bar=100 μm. G The quantification of 8-OHdG positive cells was expressed per field. There were no significant differences among the six groups. Values are expressed as mean ± SEM (error bars)

did not determine the mechanisms underlying these differences. Since the mechanisms of myocardial necrosis and apoptosis are different [15], our results do not discourage the clinical use of H_2.

On the other hand, we also observed the tendency that H_2 gas mediates the inhibitory effect on reperfusion arrhythmias suggesting that H_2 gas may primarily inhibit reperfusion lethal arrhythmias, however, we cannot deny the

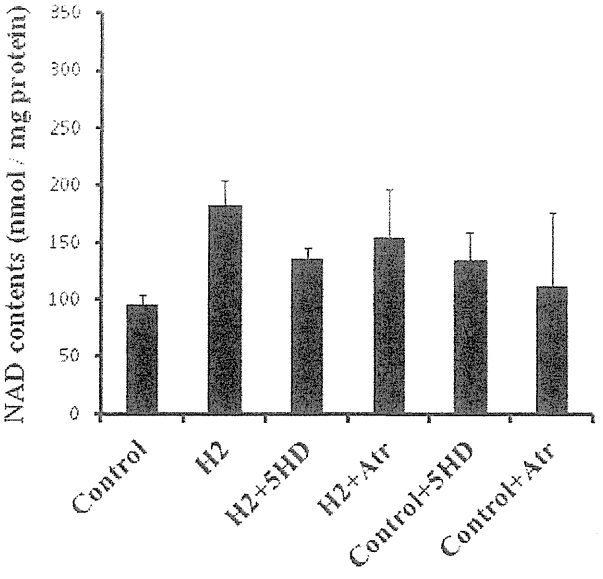

Fig. 5 The myocardial NAD contents. There were no significant differences of myocardial NAD contents among the six groups. Values are expressed as mean + SEM (error bars)

possibility that this anti-arrhythmic effect of H_2 gas is secondary to the infarct size-limiting effect.

Cellular mechanisms of H_2 gas-induced cardioprotection

H_2 gas is reported to scavenge the detrimental, hydroxyl-radical and peroxynitrate reactive oxygen species without affecting less potent oxygen derived-free radicals or hydrogen peroxide [10]. This may afford cardioprotection by attenuating the end-products of ROS [5, 16–19]. However, this does not necessarily mean that removal of detrimental ROS is the sole mechanism by which H_2 gas induces cardioprotection. Indeed, we found no significant differences in myocardial 8-OHdG immunoreactivity (Fig. 4) among the six groups although there was a trend to lower 8-OHdG positive cells, suggesting that the current dose of H_2 gas may not provide anti-oxidant effects enough to potently reduce infarct size. In turn, we observed the alternative mechanism for H_2 gas to mediate cardioprotection, i.e., the activation of mK_{ATP} followed by the inhibition of mPTP during reperfusion following myocardial ischemia. It would be difficult for chemicals or endogenous substances to physically reach mK_{ATP} upon reperfusion, and the most important endogenous mediator of ischemic preconditioning, adenosine, opens mK_{ATP} via adenosine receptors, Gi proteins, and PKC pathways [20–23]. However, H_2 gas easily penetrates cells and reaches cellular substances and mitochondria [10], suggesting that H_2 gas can reach and activate mK_{ATP}. Another possibility is that H_2 gas activates PKC inside cells, and the activated PKC opens mK_{ATP}. The activation of mK_{ATP} is reported to transmit signals that inhibit mPTP [24–30], which causes potent cardioprotection. An additional finding was that no significant differences were shown in myocardial NAD^+ contents although there was a trend to increase in H_2 group. The effects of H_2 gas to modulate either mKATP or mPTP are through a pathway other than NADH dehydrogenase, although there are data showing that the opening of mKATP increases ROS, which modulates mPTP and mediates cardioprotection.

Although we do not understand the precise mechanisms by which H_2 gas opens mK_{ATP}, the evidence in the present study suggests that H_2 gas stimulates intracellular signaling pathways of ischemic preconditioning or postconditioning of cardioprotection [31]. Since H_2 gas is produced in vivo [32], this mechanism may serve as a trigger or mediator of ischemic preconditioning. In turn, it is hard for basic and clinical researchers to translate the fruitful results of ischemic pre- or postconditioning to clinical outcomes. If H_2 gas-induced cardioprotection breaks into the sequels of the signal transduction of ischemic pre- or postconditioning, H_2 gas is likely to be used in clinical situations. Indeed, cyclosporine, which inhibits mPTP, has recently been shown to mediate potent cardioprotection in patients with acute myocardial infarction [9].

Translation to clinical medicine

Before considering the translation of the present results to clinical settings, we need to consider several issues. First, we used 1.3% H_2 gas in the present study. However, since even 0.5% H_2 gas was shown to limit infarct size in previous work [5], 1.3% or even 1% H_2 gas may be sufficient to reduce infarct size in humans. Further, it may be a good idea to use H_2 saline because several studies have shown the cytoprotective effects of H_2 saline [4, 18, 33–38]. Second, we sometimes use carperitide, nicorandil, or nitrate upon reperfusion in patients with AMI as an adjunct therapy, and these drugs might weaken the ability of H_2 gas to limit infarct size. Carperitide and nitrate have been reported to use pathways other than mK_{ATP} [39–41]; however, nicorandil may share this pathway with H_2 gas. However, since neither nicorandil nor H_2 gas fully opens mK_{ATP} channels in vivo, the combination of these two chemicals may be additive or synergistic in limiting infarct size. Third, we observed that inhalation of H_2 gas also tended to reduce the incidence of lethal ventricular arrhythmia such as ventricular tachycardia and Vf. Although we did not precisely investigate the cellular mechanisms whereby H_2 gas limited the incidence of lethal arrhythmia, we assume that the opening of mK_{ATP} and the inhibition of mPTP may be primarily or secondarily involved (Table 2).

Although we need to overcome many issues to translate the present findings, we are encouraged to further

investigate this issue by the fact that we observed H_2 gas-induced cardioprotection in large animals and the mechanism is attributable to the activation of mK_{ATP} followed by the inhibition of mPTP.

Acknowledgements This work was supported by the Grants-in-aid from the Ministry of Health, Labor, and Welfare-Japan (H23-Nanchi-Ippan-22 to M.K.) and Grants-in-aid from the Ministry of Education, Culture, Sports, Science and Technology-Japan (21390251 to M.K.) and Grants from the Japan Heart Foundation and Grants from the Japan Cardiovascular Research Foundation. The authors thank Akiko Ogai for her technical assistance; Hatsue Ishibashi-Ueda for advice about TUNEL staining and Imai Nobuyoshi for his technical assistance with TUNEL staining; Kyoko Shioya for her assistance with animal care; Toshiyasu Asahara and Masaharu Onogi (TAIYO NIPPON SANSO Co.) for providing information about hydrogen.

Conflict of interest The authors declare that they have no conflict of interest.

References

1. Ovize M, Baxter GF, Di Lisa F, et al. Postconditioning and protection from reperfusion injury: where do we stand? Position paper from the Working Group of Cellular Biology of the Heart of the European Society of Cardiology. Cardiovasc Res. 2010;87:406–23.
2. Hausenloy DJ, Baxter G, Bell R, et al. Translating novel strategies for cardioprotection: the Hatter Workshop Recommendations. Basic Res Cardiol. 2010;105:677–86.
3. Kitakaze M, Asakura M, Kim J, et al. Human atrial natriuretic peptide and nicorandil as adjuncts to reperfusion treatment for acute myocardial infarction (J-WIND): two randomised trials. Lancet. 2007;370:1483–93.
4. Sun Q, Kang Z, Cai J, et al. Hydrogen-rich saline protects myocardium against ischemia/reperfusion injury in rats. Exp Biol Med. 2009;234:1212–9.
5. Hayashida K, Sano M, Ohsawa I, et al. Inhalation of hydrogen gas reduces infarct size in the rat model of myocardial ischemia–reperfusion injury. Biochem Biophys Res Commun. 2008;373:30–5.
6. Hausenloy DJ, Ong S-B, Yellon DM. The mitochondrial permeability transition pore as a target for preconditioning and postconditioning. Basic Res Cardiol. 2009;104:189–202.
7. Di Lisa F, Canton M, Carpi A, et al. Mitochondrial injury and protection in ischemic pre- and postconditioning. Antioxid Redox Signal. 2011;14:881–91.
8. Heusch G, Boengler K, Schulz R. Inhibition of mitochondrial permeability transition pore opening: the Holy Grail of cardioprotection. Basic Res Cardiol. 2010;105:151–4.
9. Piot C, Croisille P, Staat P, et al. Effect of cyclosporine on reperfusion injury in acute myocardial infarction. N Engl J Med. 2008;359:473–81.
10. Ohsawa I, Ishikawa M, Takahashi K, et al. Hydrogen acts as a therapeutic antioxidant by selectively reducing cytotoxic oxygen radicals. Nat Med. 2007;13:688–94.
11. Kitakaze M, Node K, Minamino T, et al. Role of activation of protein kinase C in the infarct size-limiting effect of ischemic preconditioning through activation of ecto-5′-nucleotidase. Circulation. 1996;93:781–91.
12. Mori H, Haruyama S, Shinozaki Y, et al. New nonradioactive microspheres and more sensitive X-ray fluorescence to measure regional blood flow. Am J Physiol. 1992;263:H1946–57.
13. Kitakaze M, Node K, Minamino T, et al. Role of nitric oxide in regulation of coronary blood flow during myocardial ischemia in dogs. J Am Coll Cardiol. 1996;27:1804–12.
14. Kitakaze M, Node K, Takashima S, et al. Role of cellular acidosis in production of nitric oxide in canine ischemic myocardium. J Mol Cell Cardiol. 2001;33:1727–37.
15. Kung G, Konstantinidis K, Kitsis RN. Programmed necrosis, not apoptosis, in the heart. Circ Res. 2011;108:1017–36.
16. Fukuda K-I, Asoh S, Ishikawa M, Yamamoto Y, Ohsawa I, Ohta S. Inhalation of hydrogen gas suppresses hepatic injury caused by ischemia/reperfusion through reducing oxidative stress. Biochem Biophys Res Commun. 2007;361:670–4.
17. Buchholz BM, Kaczorowski DJ, Sugimoto R, et al. Hydrogen inhalation ameliorates oxidative stress in transplantation induced intestinal graft injury. Am J Transplant. 2008;8:2015–24.
18. Cai J, Kang Z, Liu K, et al. Neuroprotective effects of hydrogen saline in neonatal hypoxia–ischemia rat model. Brain Res. 2009;1256:129–37.
19. Li J, Wang C, Zhang JH, Cai JM, Cao YP, Sun XJ. Hydrogen-rich saline improves memory function in a rat model of amyloid-beta-induced Alzheimer's disease by reduction of oxidative stress. Brain Res. 2010;1328:152–61.
20. Tsukamoto O, Asanuma H, Kim J, et al. A role of opening of mitochondrial ATP-sensitive potassium channels in the infarct size-limiting effect of ischemic preconditioning via activation of protein kinase C in the canine heart. Biochem Biophys Res Commun. 2005;338:1460–6.
21. Hanley P, Daut J. K channels and preconditioning: a re-examination of the role of mitochondrial K channels and an overview of alternative mechanisms. J Mol Cell Cardiol. 2005;39:17–50.
22. Kitakaze M, Minamino T, Node K, et al. Role of activation of ectosolic 5′-nucleotidase in the cardioprotection mediated by opening of K+c channels. Am J Physiol. 1996;270:H1744–56.
23. O'Rourke B. Myocardial K(ATP) channels in preconditioning. Circ Res. 2000;87:845–55.
24. Hausenloy DJ, Maddock HL, Baxter GF, Yellon DM. Inhibiting mitochondrial permeability transition pore opening: a new paradigm for myocardial preconditioning? Cardiovasc Res. 2002;55:534–43.
25. Lim SY, Davidson SM, Hausenloy DJ, Yellon DM. Preconditioning and postconditioning: the essential role of the mitochondrial permeability transition pore. Cardiovasc Res. 2007;75:530–5.
26. Murata M, Akao M, O'Rourke B, Marban E. Mitochondrial ATP-sensitive potassium channels attenuate matrix Ca2+ overload during simulated ischemia and reperfusion: possible mechanism of cardioprotection. Circ Res. 2001;89:891–8.
27. Hausenloy DJ. Preconditioning protects by inhibiting the mitochondrial permeability transition. AJP Heart Circ Physiol. 2004;287:H841–9.
28. Costa ADT. The mechanism by which the mitochondrial ATP-sensitive K+ channel opening and H2O2 inhibit the mitochondrial permeability transition. J Biol Chem. 2006;281:20801–8.
29. Juhaszova M, Zorov DB, Kim SH, et al. Glycogen synthase kinase-3beta mediates convergence of protection signaling to inhibit the mitochondrial permeability transition pore. J Clin Invest. 2004;113:1535–49.
30. Terashima Y, Sato T, Yano T, et al. Roles of phospho-GSK-3β in myocardial protection afforded by activation of the mitochondrial KATP channel. J Mol Cell Cardiol. 2010;49:762–70.
31. Heusch G, Boengler K, Schulz R. Cardioprotection: nitric oxide, protein kinases, and mitochondria. Circulation. 2008;118:1915–9.
32. Hammer HF. Colonic hydrogen absorption: quantification of its effect on hydrogen accumulation caused by bacterial fermentation of carbohydrates. Gut. 1993;34:818–22.

33. Chen H, Sun YP, Hu PF, et al. The effects of hydrogen-rich saline on the contractile and structural changes of intestine induced by ischemia-reperfusion in rats. J Surg Res. 2011;167:316–22.
34. Mao YF, Zheng XF, Cai JM, et al. Hydrogen-rich saline reduces lung injury induced by intestinal ischemia/reperfusion in rats. Biochem Biophys Res Commun. 2009;381:602–5.
35. Wang F, Yu G, Liu SY, et al. Hydrogen-rich saline protects against renal ischemia/reperfusion injury in rats. J Surg Res. 2011;167:e339–44.
36. Liu Q, Shen WF, Sun HY, et al. Hydrogen-rich saline protects against liver injury in rats with obstructive jaundice. Liver Int. 2010;30:958–68.
37. Chen C, Chen Q, Mao Y, et al. Hydrogen-rich saline protects against spinal cord injury in rats. Neurochem Res. 2010;35:1111–8.
38. Zheng X, Mao Y, Cai J, et al. Hydrogen-rich saline protects against intestinal ischemia/reperfusion injury in rats. Free Radic Res. 2009;43:478–84.
39. John SW, Krege JH, Oliver PM, et al. Genetic decreases in atrial natriuretic peptide and salt-sensitive hypertension. Science. 1995;267:679–81.
40. Ignarro LJ, Buga GM, Wood KS, Byrns RE, Chaudhuri G. Endothelium-derived relaxing factor produced and released from artery and vein is nitric oxide. Proc Natl Acad Sci U S A. 1987;84:9265–9.
41. Murad F. Cellular signaling with nitric oxide and cyclic GMP. Braz J Med Biol Res. 1999;32:1317–27.

Journal of Controlled Release 160 (2012) 274–280

Contents lists available at SciVerse ScienceDirect

Journal of Controlled Release

journal homepage: www.elsevier.com/locate/jconrel

Development of anti-HB-EGF immunoliposomes for the treatment of breast cancer

Kaoru Nishikawa [a], Tomohiro Asai [a], Hirokazu Shigematsu [a], Kosuke Shimizu [a], Hisakazu Kato [b], Yoshihiro Asano [b], Seiji Takashima [b], Eisuke Mekada [c], Naoto Oku [a], Tetsuo Minamino [b,*]

[a] Department of Medical Biochemistry and Global COE Program, School of Pharmaceutical Sciences, University of Shizuoka, 52-1 Yada, Suruga-ku, Shizuoka 422-8526, Japan
[b] Department of Cardiovascular Medicine, Osaka University Graduate School of Medicine, Suita, Osaka 565-0871, Japan
[c] Department of Cell Biology, Research Institute for Microbial Diseases, Osaka University, Suita, Osaka 565-0871, Japan

ARTICLE INFO

Article history:
Received 22 August 2011
Accepted 8 October 2011
Available online 14 October 2011

Keywords:
HB-EGF
immunoliposome
breast cancer

ABSTRACT

Increased expression of heparin-binding epidermal growth factor-like growth factor (HB-EGF) is frequently observed in certain cancers such as ovarian and breast cancers, and this protein is a desirable target for drug delivery by a drug delivery system (DDS). In the present study, we developed novel immunoliposomes targeting HB-EGF for cancer therapy. The immunoliposomes significantly associated with Vero-H cells overexpressing HB-EGF compared with their binding to wild-type Vero cells, whereas liposomes without modification by the antibody did not associate with either type of cells. Moreover, enhanced uptake of the immunoliposomes into Vero-H cells was observed as well as that into MDA-MB-231 human breast cancer cells, which are known to highly express HB-EGF. These results suggest that HB-EGF mediates the binding and uptake of the immunoliposomes in HB-EGF-expressing cells. Next, we determined the therapeutic effect of these immunoliposomes encapsulating an anticancer drug on tumor-bearing mice. For this purpose, we prepared doxorubicin (DOX)-encapsulated immunoliposomes and injected them intravenously into mice bearing MDA-MB-231 cancer cells. As a result, these DOX-encapsulated immunoliposomes suppressed not only tumor progression but also tumor regression. In conclusion, our results indicate that anti-HB-EGF antibody-modified liposomes could be a useful DDS carrier for the treatment of HB-EGF-expressing cancers.

1. Introduction

Heparin-binding epidermal growth factor-like growth factor (HB-EGF) is known to stimulate the growth of various cells in an autocrine or a paracrine manner. This protein is highly expressed on various cancer cells, such as those of ovarian and breast cancer [1,2], and is also expressed on tumor angiogenic vessels [3,4]. Therefore, HB-EGF seems to be a target molecule for the treatment of certain cancers. In fact, CRM197, which binds to the EGF-domain of HB-EGF and prevents HB-EGF from binding to ErbB receptors and therefore regulates the cell proliferation, is now under clinical trials [5]. The usefulness of HB-EGF as a molecular target of cancer treatment has been suggested in several reviews [6–8]. Although HB-EGF can be produced as a membrane-anchored form (proHB-EGF) and later processed to its soluble form, a significant amount of proHB-EGF remains on the cell surface [9]. Therefore, HB-EGF might be also a useful target molecule for drug delivery via a DDS to tumors and tumor angiogenic vessels.

In the present study, we aimed at delivering an anticancer drug to HB-EGF-expressing cancer cells by use of liposomes as a drug carrier. Polyethylene glycol (PEG)-modified liposomes have been the most widely investigated as carriers of drugs and molecules having biological activities, since PEG forms an aqueous layer on the liposomal surface that avoids reticuloendothelial system (RES) trapping of the liposomes [10,11]. PEGylated liposomes have a relatively long circulation time and tend to accumulate in tumor tissues through leaky angiogenic vessels, a phenomenon referred to as the enhanced permeability and retention (EPR) effect [12,13]. Moreover, liposomalization can reduce off-target toxicity of the drugs encapsulated [14]. In fact, PEG-modified liposomes containing doxorubicin (DOX) have been used in clinical cancer therapy. On the other hand, actively targeted liposomes decorated with ligands such as antibodies [15,16], proteins such as transferrin [17], and peptides [18–20] achieve more selective drug delivery to tumor tissues. These ligands that recognize tumor- or tumor angiogenic vessel-associated molecules are conjugated to the head of the PEG-chain of liposomes.

Herein, we decorated DOX-loaded liposomes with anti-HB-EGF antibody and evaluated the systemic and targeted delivery of DOX to cancer cells in breast cancer-bearing mice. The results indicate that this immunoliposomal DOX significantly suppressed tumor growth in comparison with non-modified PEG-liposomal DOX. Our findings suggest that targeted delivery of anti-HB-EGF-modified PEGylated liposomes could be a useful carrier of doxorubicin for the treatment of HB-EGF-expressing cancers.

* Corresponding author. Tel.: +81 6 6879 3635; fax: +81 6 6879 3645.
E-mail address: tminamino@cardiology.med.osaka-u.ac.jp (T. Minamino).

0168-3659/$ – see front matter © 2011 Elsevier B.V. All rights reserved.
doi:10.1016/j.jconrel.2011.10.010

2. Materials and Methods

2.1. Materials

Anti-human HB-EGF monoclonal antibody (IgG) was ordered and received from Medical and Biological Laboratories Co. Ltd. The monoclonal antibody clone 3E9 specific for HB-EGF was obtained by the method described previously [21]. The 3E9 clone recognized the EGF-like domain of human proHB-EGF, but not that of mouse proHB-EGF. Hydrogenated soy phosphatidylcholine (HSPC), methoxy-polyethyleneglycol 2000-conjugated distearoylphosphatidylethanolamine (DSPE-PEG), and cholesterol were gifts from Nippon Fine Chemical Co. Ltd. (Kobe, Japan). DSPE-PEG-maleimide (SUNBRIGHT DSPE-0.20MA) was obtained from NOF Co. Ltd. (Tokyo, Japan). 1,1'-Dioctadecyl- 3,3,3',3',-tetramethylindocarbocyanine perchlorate ($DiIC_{18}$) was purchased from Molecular Probes, Inc. (Eugene, OR).

2.2. Preparation of Fab' of anti-HB-EGF monoclonal antibody

Stock solution of anti-HB-EGF IgG was applied onto a PD-10 column (GE Healthcare, UK., Ltd., Buckinghamshire) to exchange the solvent for 100 mM sodium citrate buffer, pH 3.5 (100 mg IgG/20 mL). To eliminate the Fc region of the IgG, pepsin (from porcine gastric mucosa, Sigma-Aldrich) solution (final concentration of 0.01% w/v) was added to the antibody solution and incubated the mixture at 37 °C for 3 h, after which the reaction was stopped by the addition of a 10% volume of 3 M Tris–HCl (pH 7.5). The generated $F(ab')_2$ was washed twice with 100 mM sodium phosphate buffer, pH 6.0, and concentrated by ultrafiltration (5,000 *g* for 20 min) with an Amicon® Ultra-4 (10,000 NMWL, Millipore). Ten milligrams aliquot of $F(ab')_2$ was diluted with 100 mM sodium phosphate buffer, and 0.1 mL of 100 mM cysteamine hydrochloride was added to a final volume of 1 mL, followed by incubation at 37 °C for 90 min. Then, the reaction solution was purified by gel-filtration chromatography (1.0 cm×50 cm, Ultrogel AcA, PALL Life Sciences), and the Fab' fraction was collected with a fraction collector. The Fab' fraction was concentrated by ultrafiltration (5,000 *g* for 30 min) with Amicon Ultra-4 (10,000 NMWL).

2.3. Preparation of plain liposomes

Liposomes were prepared by thin lipid-film hydration followed by vortexing and sonication. In brief, 20 μmol HSPC and 10 μmol cholesterol dissolved in chloroform were transferred to a round-bottomed flask, evaporated until a thin lipid film had formed on a rotary evaporator under reduced pressure, and stored *in vacuo* for at least 1 h. The dried film was hydrated with 2 mL of saline, warmed at 65 °C in a water bath, vortexed until the lipids had become detached from the side of the flask, and sonicated with a bath-type sonicator at 65 °C. Three cycles of the following were performed: freezing of the liposomal solution in the flask with liquid nitrogen, thawing at room temperature, incubating at 65 °C in a water bath for 5 min, and vortexing for 30 s. Then, the liposomes were filtered through polycarbonate membrane filters having 100-nm-diameter pores by use of an Extruder (Lipex, Vancouver) at 65 °C. Finally, the liposome solution was diluted with saline; and the liposomal pellet was collected after ultracentrifugation (450,000 g×1 h, CS120GXL, Hitachi) and resuspended in 2 mL of saline.

For the fluorescence-labeling of liposomes, HSPC, cholesterol, and $DiIC_{18}$ (2:1:0.1 as a molar ratio) dissolved in chloroform were used for preparing a thin lipid film. Further preparation was essentially the same as described above except that all procedures were done under shading from ambient light.

For the encapsulation of DOX into the liposomes, the thin lipid film was hydrated in 250 mM ammonium sulfate (pH 5.5) instead of saline; and after freeze-thawing, extrusion for sizing, and centrifugation, the liposomes resuspended in saline was incubated in the presence of 1.8 mg/mL DOX at 65 °C for 1 h. Untrapped DOX was removed by ultracentrifugation, and the liposomal pellet was resusupended in saline (final concentration of 10 mM as DSPC). The encapsulation efficiency of DOX was calculated based on the amount of untrapped DOX and liposomal DOX after the addition of Triton X-100, with DOX quantified at 484-nm absorbance.

2.4. Surface decoration of liposomes with PEG or anti-HB-EGF antibody-PEG

DSPE-PEG (MPEG-2000-DSPE) and DSPE-PEG-maleimide were dissolved in saline to a final concentration of 10 mM each. One milliliter of plain liposomes (10 mM as DSPC) prepared as described above were incubated at 65 °C for 15 min after addition 100 μL of DSPE-PEG or DSPE-PEG-maleimide to obtain PEG-modified liposomes (PEG-Lip) and PEG-maleimide-modified liposomes.

The coupling of Fab' with the maleimide moiety of PEG-maleimide-modified liposomes was performed according to the method described previously [22], with the following modification: Fab' and PEG-maleimide-modified liposomes (1:1 molar ratio of Fab' and maleimide moiety) were mixed, and the coupling reaction was carried out at 4 °C for 20 h. Excess Fab' was separated from the Fab'-coupled liposomes by use of Sepharose 4 Fast Flow gel filtration, and the liposomal fraction was collected. After ultracentrifugation at 450,000 g, 4 °C for 1 h (CS120GXL, Hitachi), the liposomal pellet was resuspended in 1 mL of saline.

Liposome size and ζ-potential were determined with a Zeta Sizer (Nano –ZS, Malvern Instruments, Worcs, UK).

2.5. Cells and cell culture

Vero cells derived from African green monkey's kidney were cultured in MEM medium (GIBCO) supplemented with 10% fetal bovine serum (FBS; Sigma-Aldrich), 100 units/mL penicillin G (MP Biomedicals, Irvine, CA), and 100 μg/mL streptomycin (MP Biomedicals) in a CO_2 incubator. Vero-H cells isolated by transfection with human HB-EGF cDNA [23] were cultured similarly except that the medium was supplemented with 1 μg/mL G418.

MDA-MB-231 human breast cancer cells were cultured in Leibovitz L-15 medium (GIBCO) supplemented with 10% FBS, 100 units/mL penicillin G, and 100 μg/mL streptomycin in a CO_2 incubator.

2.6. Real-time PCR

Vero, Vero-H, and MDA-MB-231 cells were cultured on a 60-mm culture dish for 24 h and washed with ice-cold PBS for three times. Then, the cells were collected by a scraper; and total RNA was extracted with RNeasy Plus Mini Kit (QIAGEN) according to the manufacturer's instruction. Then cDNA was generated from the total RNA samples (4 μg) by using a Ready-To-Go T-Primed First-Strand Kit (GE Healthcare). In the presence of human HB-EGF or β-actin primer (Takara Bio Inc. Shiga, Japan), and SYBR Premix Ex Taq II (Takara Bio), real-time PCR was performed with a Thermal Cycler Dice Real Time System (Takara Bio). The PCR conditions were the following: 95 °C for 30 sec, followed by 40 cycles of 95 °C for 5 sec, 60 °C for 30 sec; 95 °C for 15 sec, 60 °C for 30 sec, and 95 °C for 15 sec.

2.7. Western blotting

Vero, Vero-H, and MDA-MB-231 cells were cultured on a 60-mm culture dish for 24 h and washed with ice-cold PBS for three times. Then, the cells were solubilized in lysis buffer (50 mM Tris–HCl [pH7.4] containing 1% Triton-X, 150 mM NaCl, and protease inhibitors [2 mM PMSF, 50 μg/mL aprotinin, 50 μg/mL pepstatin, and 0.2 mM leupeptin]). The supernatant of the cell lysate was collected and suspended in loading buffer (16 mM Tris–HCl, 2.5% glycerol, 0.5% SDS, 200 mM 2-mercaptoethanol, 0.001% bromophenol blue; pH 6.8).

Immediately after having been heated at 95 °C for 5 min, the sample was subjected to reducing SDS-PAGE on 10% acrylamide gel. Protein concentrations were measured by using a BCA Protein Assay Reagent Kit (PIERCE Biotechnology, Rockford, IL).

After separation by SDS-PAGE, proteins were transferred electrophoretically (40 V, 90 min) to a PVDF membrane (Bio-Rad). After having been blocked with 3% BSA in TBS/Tween 20 buffer (TBS/T: 50 mM Tris HCl [pH 7.4] containing 150 mM NaCl and 0.05% Tween 20), the blots were incubated at 25 °C for 1 h with goat polyclonal anti-HB-EGF antibody (1:2,000 solution, R&D systems) for the detection of HB-EGF. The membrane was washed thrice with TBS/T, and was probed for 60 min at 25 °C with donkey anti-goat horseradish peroxidase-conjugated secondary antibody (1:4,000 dilution). The probed membranes were washed 3 times (10 min each time) with TBS/T, and immunoreactive proteins were detected by using the enhanced chemiluminescence method.

2.8. Binding to and uptake of Ab-PEG-Lip into various cells

Vero, Vero-H, and MDA-MB-231 cells were cultured in a 24-well plate (2×10^4 cells/500 μL/well) at 37 °C for 48 h. After removal of the medium, $DiIC_{18}$-labeled PEG-Lip or Ab-labeled PEG-Lip (0.05 to 0.2 mM as DSPC) was added to the well; and the cells were then incubated at 4 °C or 37 °C. Next, the cells were washed thrice with cold PBS and solubilized with 10 mM Tris buffer, pH 7.4, containing 0.1% SDS. The samples were diluted 200-fold with 10 mM Tris buffer, pH 7.4, containing 0.1% SDS; and aliquots were transferred to a 96-well black plate. The fluorescence intensity was monitored with a multiplate reader (Infinite M200, Tecan), with excitation and emission wave lengths of 549 nm and 592 nm, respectively. The amount of $DiIC_{18}$ associated with the cells was calculated from the standard curve.

2.9. Cell proliferation assay

MDA-MB-231 cells were seeded (2×10^4 cells/well) into a 24-well plate and incubated overnight in a CO_2 incubator. After a change of the medium, the cells were incubated at 37 °C for 4 h in the presence of DOX-encapsulated anti-HB-EGF-decorated immunoliposomes (Ab-PEG-LipDOX), DOX-encapsulated PEG-liposomes (PEG-LipDOX) or free DOX. Then, the viability of the cells was measured with TetraColorOne™ (Seikagaku, Tokyo, Japan) according to the manufacturer's instruction.

2.10. Therapeutic experiment

MDA-MB-231 cells were subcutaneously implanted (8×10^6 cells/0.2 mL/mouse) into 17-week-old BALB/C nu/nu female mice (Japan SLC Inc., Shizuoka, Japan). Then, saline (control), PEG-LipDOX or Ab-PEG-LipDOX was intravenously injected once a week for 3 weeks, on days 14, 21, and day 28 after tumor implantation. The amount of DOX injected was 10 mg/kg each time and; therefore, a total of 30 mg/kg DOX was injected. The tumor size and body weight were monitored daily from day 12 after tumor implantation. Tumor volume was calculated from the following formula:

$$\text{Tumor volume} = 0.4 \times a \times b^2 \quad (a: \text{largest diameter}, b: \text{smallest diameter})$$

The animals were cared for according to the Animal Facility Guidelines of the University of Shizuoka. All animal experiments were approved by the Animal and Ethics Committee of the University of Shizuoka.

Table 1
Particle size and ζ-potential of liposomes.

Liposomes	Size (nm)	ζ-potential (mV)
PEG-Lip	136	-0.03
PEG-LipDOX	139	-3.30
Ab-PEG-Lip	134	-3.02
Ab-PEG-LipDOX	142	-2.94

2.11. Statistical analysis

Differences between groups were evaluated by analysis of variance (ANOVA) with the Tukey *post-hoc* test.

3. Results

3.1. Characterization of Ab-PEG-Lip and Ab-PEG-LipDOX

At first, we examined the characteristics of anti-HB-EGF antibody-modified liposomes (Ab-PEG-Lip) and DOX-loaded Ab-PEG-Lip (Ab-PEG-LipDOX). As shown in Table 1, all liposomal preparations showed similar sizes, about 140 nm, and had almost neutral charges. The efficiency of conjugation of the Fab' fragment of anti-HB-EGF antibody to liposomal PEG-maleimide was determined by the protein amount before and after the conjugation reaction. When 1.94 mg Fab' had been applied on the liposomes, 1.31 mg Fab' was recovered in the

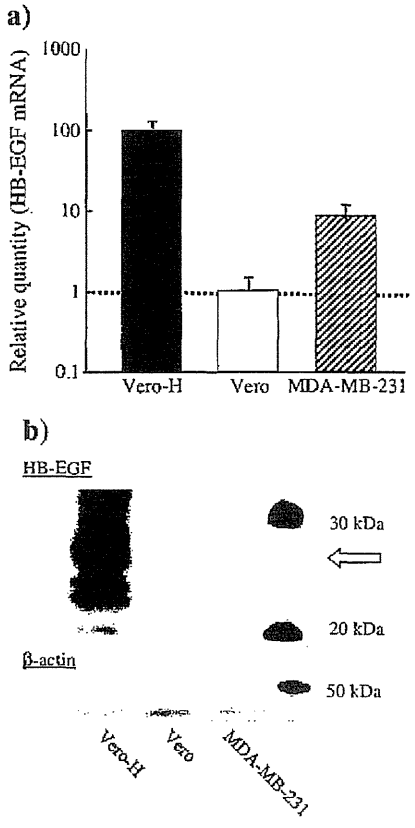

Fig. 1. Expression of HB-EGF and its transcript in various cell lines. a) Relative expression of HB-EGF mRNA was determined by real-time PCR. Total RNA was extracted from Vero, Vero-H, and MDA-MB-231 cells; and then real- time PCR for HB-EGF and β-actin was performed as described in Materials and Methods. b) Western blotting was performed on Vero, Vero-H, and MDA-MB-231 cells. The arrow indicates the position of HB-EGF. Total proteins (14 μg/sample) were fractionated by 10% SDS-PAGE. Following electrophoresis, the proteins were transferred to a PVDF membrane, and Western blotting was performed as described in Materials and Methods.

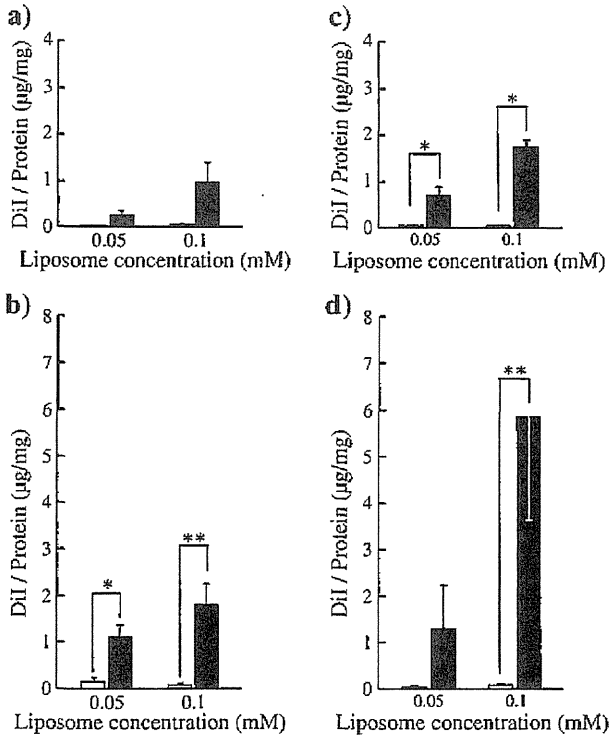

Fig. 2. Binding to and uptake of anti-HB-EGF antibody-modified liposomes into Vero and Vero-H cells. $DiIC_{18}$-labeled PEG-Lip (open columns) and Ab-PEG-Lip (closed columns) were incubated with Vero (a, c) or Vero-H (b, d) cells at 4 °C (a, b) or at 37 °C (c, d) for 4 h. The amount of liposomes bound to Vero or Vero-H cells was determined fluorometrically. Liposomes bound to Vero or Vero-H cells are presented as the amount of $DiIC_{18}$ per amount of cellular protein. Data show the mean values and S.D. (n=3). Significant differences are shown with asterisks: * $p<0.05$ and ** $p<0.01$, as indicated by the brackets or *versus* corresponding value for PEG-Lip.

liposomal fraction, indicating that the conjugation efficiency was about 67%. The encapsulation efficiency of DOX in PEG-LipDOX and Ab-PEG-LipDOX was 88.2±6.9% and 88.4±4.3%, respectively. These data indicate that the conjugation of Fab' to liposomes and DOX loading were successfully achieved.

3.2. Binding to and uptake of anti-HB-EGF immunoliposomes by HB-EGF-expressing cells

Before examining the cellular-association aspect of Ab-PEG-Lip, we assessed the expression levels of HB-EGF on Vero cells, Vero-H cells, and MDA-MB-231 cells by performing real-time PCR and Western blotting. Quite high expression of HB-EGF on Vero-H cells was confirmed by both real-time PCR (Fig. 1a) and Western blotting (Fig. 1b). Also, substantial amounts of HB-EGF mRNA and protein were expressed on MDA-MB-231 cells. In the case of Vero cells, the expression level of HB-EGF mRNA was about 100-fold less than that in Vero-H cells; and only a light band was detected by Western blotting.

The association of Ab-PEG-Lip with Vero, Vero-H, and MDA-MB-231 cells was examined for evaluating the targeting effectiveness of the liposomes. Ab-PEG-Lip bound more to Vero-H cells than to Vero cells (Fig. 2a, b). Moreover, the amount of the immunoliposomes taken up into cells was greater for Vero-H cells than for Vero cells. Most of the liposome-associated label (DiI) had probably been taken up into the cells at 37 °C, although some of it may have remained bound to the surface of the cells.

Next the uptake of Ab-PEG-Lip into human breast cancer cells was investigated by using MDA-MB-231 cells, which had been confirmed by real-time PCR and Western blotting (Fig. 1) to have high expression of HB-EGF protein. Ab-PEG-Lip was significantly taken up into the MDA-MB-231 cells at 37 °C(Fig. 3). These data would also include the liposomes bound to the cells. Therefore, these immunoliposomes bound to and were taken up specifically into the HB-EGF-expressing breast-cancer cells, indicating that they could be a useful carrier for drug delivery.

3.3. Antiproliferative effect of DOX encapsulated in anti-HB-EGF immunoliposomes on HB-EGF-expressing cells

Next, the anti-proliferative effect of DOX encapsulated in Ab-PEG-Lip on MDA-MB-231 cells as well as on Vero-H cells was examined. As shown in Fig. 4, the immunoliposomal formulation of DOX suppressed the growth of both MDA-MB-231 and Vero-H cells in a

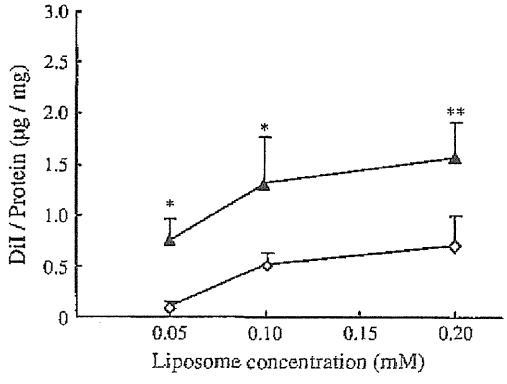

Fig. 3. Association of anti-HB-EGF antibody-modified liposomes with MDA-MB-231 cells. MDA-MB-231 cells were incubated with $DiIC_{18}$-labeled PEG-Lip (◇) or Ab-PEG-Lip (▲) at 37 °C for 4 h. After the cells had been washed with PBS, the amount of liposomes associated with them was determined fluorometrically. Amounts of bound/internalized liposomes are presented as the amount of $DiIC_{18}$ per amount of MDA-MB-231 cell protein. Data show the mean values and S.D. (n=3). Significant differences are shown with asterisks: * $p<0.05$ and ** $p<0.01$ *versus* corresponding value for PEG-Lip.